The Astrophysical Journal, 665:1391–1406, 2007 August 20


# THE DISK AND ENVIRONMENT OF A YOUNG VEGA ANALOG: HD 169142

C. A. Grady,[1,2] G. Schneider,[3] K. Hamaguchi,[4,5] M. L. Sitko,[6,7] W. J. Carpenter,[7] D. Hines,[6] K. A. Collins,[8,9] G. M. Williger,[8,10] B. E. Woodgate,[2] Th. Henning,[11] F. Ménard,[12] D. Wilner,[13] R. Petre,[14] P. Palunas,[15] A. Quirrenbach,[16] J. A. Nuth III,[17] M. D. Silverstone,[3] and J. S. Kim[3]

*Received 2006 November 6; accepted 2007 May 10*

## ABSTRACT

We trace the disk of HD 169142 (A8 Ve) from 0.57″ to 1.4″ (≈80–200 AU projected distance) in 1.1 $\mu$m scattered light with *HST* NICMOS coronagraphy. The azimuthally symmetric disk has a peak azimuthally medianed surface brightness (SB) of ≈5 mJy arcsec$^{-2}$ at 0.57″ from the star, and drops $\propto r^{-3}$. This radial SB profile is consistent with the presence of spatially resolved PAH emission and a Meeus group I IR SED only if the inner disk is either substantially flatter than the outer disk or partially devoid of material. Analysis of new *HST* ACS FUV imagery in tandem with archival *IUE* data indicates $\dot{M}_{\rm acc} \leq 10^{-9}\,M_{\odot}$ yr$^{-1}$. We estimate the age of HD 169142 to be $6^{+6}_{-3}$ Myr by identifying 2MASS 18242929−2946559, located 9.3″ to the southwest, as a 130 mas separation weak-line T Tauri binary that is comoving with HD 169142 at the 4 $\sigma$ confidence level. We find no evidence for any additional *stellar* companion in either the ACS or *Chandra* ACIS-S data at $r \leq 1''$. HD 169142 has previously been interpreted as a slowly rotating, chemically peculiar star. However, by combining the disk inclination and $v \sin i$ from the literature, we find that the star has $v_{\rm equatorial} \approx 240$ km s$^{-1}$, making it a rapid rotator, similar to Altair or Vega. The UV data for HD 169142 are consistent with gravity darkening, while the X-ray luminosity and spectrum resembles early F stars at the age of the $\beta$ Pictoris moving group, rather than mid-A stars. In this context, spectral features previously interpreted as evidence for chemical peculiarity are more likely to reflect the presence of a strong photospheric latitudinal temperature gradient. With such a gradient, HD 169142 should closely resemble Vega at the epoch of central disk clearing.

*Subject headings:* binaries: visual — planetary systems: protoplanetary disks — stars: individual (2MASS 18242929−2946559, HD 22128, HD 36112, HD 142666, HD 169142, HD 220750) — stars: low-mass, brown dwarfs — stars: pre–main-sequence

## 1. INTRODUCTION

One of the predicted steps in the evolution of a planetary system is central clearing of the disk. Two principal mechanisms for clearing have been proposed: (1) photoevaporation of the gaseous content of the inner disk (Alexander et al. 2006), and (2) dynamical sculpting by giant planets (Augereau & Papaloizou 2004). In both cases, the removal of the bulk of the gas from the inner disk directly constrains the time available for giant planet formation and migration. As a result, "transitional" disks (Strom & Najita 2005), deficient in warm, near-stellar dust and gas but harboring abundant material at larger radii, are of interest, particularly if they can be securely dated. Currently, our most detailed knowledge of protoplanetary disks is limited to nearby and typically isolated objects. Age estimates have proven problematic for most A stars due to the rapid evolution of the star to the zero-age main sequence, with reliable dating of isolated A stars difficult after ≈5 Myr (Stauffer 2004). However, the identification of comoving groups of low-mass stars that are associated with A stars (e.g., Zuckerman & Song 2004) permits independent dating of the A star. On smaller scales, the combination of high angular resolution imaging and multiwavelength data has revealed low-mass common-proper- motion companions to several Herbig Ae stars (e.g., Weinberger et al. 2000; Grady et al. 2004; Feigelson et al. 2006; Chen et al. 2006; Carmona et al. 2007).

HD 169142 ($J = 7.310, H = 6.911, K = 6.410$),[18] is a Herbig Ae star that was first identified as having circumstellar material by Walker & Wolstencroft (1988). Subsequently, the mid-IR spectrum indicated that the circumstellar environment of HD 169142 has very little warm dust, compared to expectations for protoplanetary disks. The mid-IR spectrum has conspicuous emission in the C−H bending and stretching modes associated with polycyclic aromatic hydrocarbons (PAHs), together with an absence of emission from small, warm silicates (Sylvester

[1] Eureka Scientific, 2452 Delmer, Suite 100, Oakland, CA 96002.
[2] ExoPlanets and Stellar Astrophysics Laboratory, Code 667, NASA's Goddard Space Flight Center, Greenbelt, MD 20771.
[3] Steward Observatory, University of Arizona, Tucson, AZ 85721.
[4] Universities Space Research Association, Columbia, MD 21044-3432.
[5] Astrophysics Science Division, NASA's Goddard Space Flight Center, Greenbelt, MD 20771.
[6] Space Science Institute, 4750 Walnut Street, Suite 205, Boulder, CO 80301.
[7] Department of Physics, University of Cincinnati, Cincinnati, OH 45221-0011.
[8] Department of Physics, University of Louisville, Louisville, KY 40292.
[9] Supported by the Kentucky Space Grant Consortium and NASA.
[10] Department of Physics and Astronomy, Johns Hopkins University, Baltimore, MD 21218-2686.
[11] Max-Planck-Institut für Astronomie, Königstuhl 17, D-69117 Heidelberg, Germany.
[12] Laboratoire d'Astrophysique de Grenoble, CNRS/UJF UMR 5571, France.
[13] Harvard-Smithsonian Center for Astrophysics, MS 42, 60 Garden Street, Cambridge, MA 02138.
[14] Laboratory for High Energy Astrophysics, Code 666, NASA's Goddard Space Flight Center, Greenbelt, MD 20771.
[15] McDonald Observatory, University of Texas, 1 University Station, C1402, Austin, TX 78712-0259.
[16] Landessternwarte, Zentrum für Astronomie (ZAH), Universität Heidelberg, Königstuhl 12, D-69117 Heidelberg, Germany.
[17] Cosmochemistry Branch, Code 691, NASA's Goddard Space Flight Center, Greenbelt, MD 20771.

[18] Vizier Online Data Catalog, 2246 (R. M. Cutri et al., 2003).

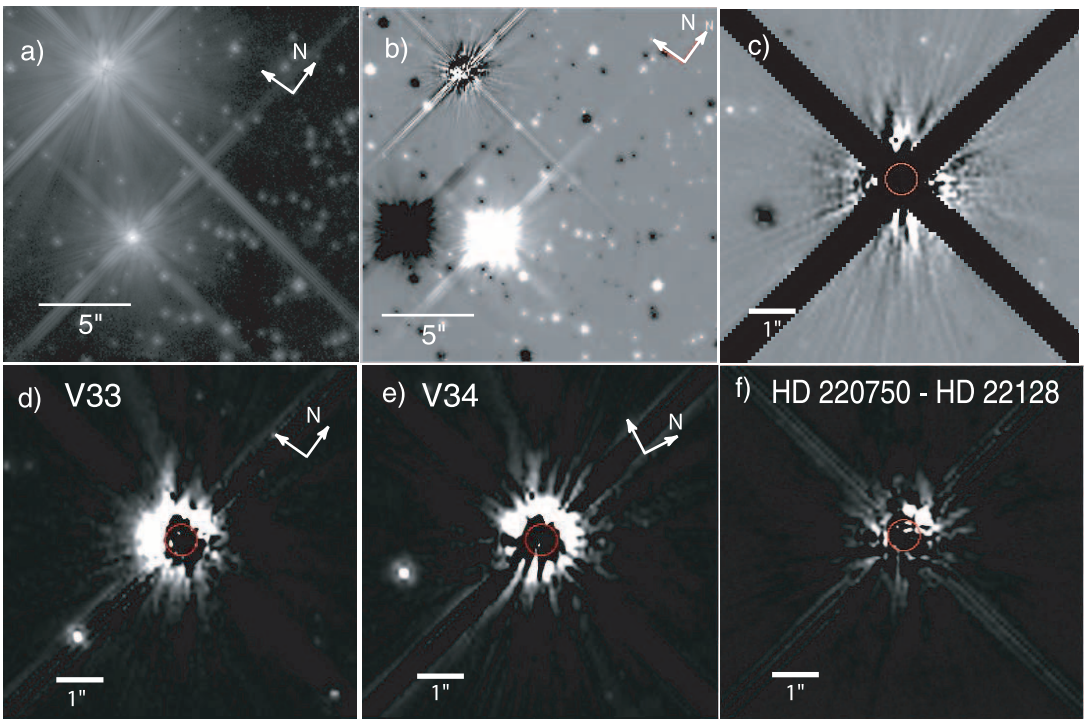


FIG. 1.—HD 169142 at 1.1 $\mu$m (F110W) as seen by NICMOS. (*a*) The Herbig Ae star (*upper left*) and 2MASS 18242929−2946559 (2M1824) are the brightest objects in the $19.2'' \times 19.3''$ NIC2 field of view. (*b*) Roll-differencing results in PSF subtraction residuals typical for the stability of the *HST*+NICMOS PSF, with no indication of nonaxisymmetric nebulosity. (*c*) Detail of the roll-differenced data showing both background stars at $r \geq 2''$ and the symmetric residuals typical of either a disk null detection or a face-on system. The data for (*b*) and (*c*) are shown with a linear stretch between −5 and 5 instrumental counts $s^{-1}$ $pixel^{-1}$ (ADU), which corresponds to a surface brightness range of $\pm 1$ mJy $arcsec^{-2}$. After subtraction of color and breathing matched median PSF template observations, excess light is seen for (*d*) visit 33, (*e*) visit 34, and (*f*) at a level that is distinctly higher than for color-matched PSF subtractions. The data for (*d*, *e*) are shown with a linear stretch between 0 and 5 mJy $arcsec^{-2}$, with white for SB $>$ 1 mJy $arcsec^{-2}$.

et al. 1996; Meeus et al. 2001; Acke & van den Ancker 2004; Sloan et al. 2005). Single-dish millimeter observations (Dent et al. 2005) have shown that the CO content of the disk is intermediate between those of the majority of Herbig Ae stars and debris disks, while the outer disk still retains sufficient CO and dust to be resolved out to $r = 1.6''$ (Raman et al. 2006). Light polarized by the disk grains was differentially detected to $r = 1.5''$ in $H$ band (Kuhn et al. 2001) and to $1.2''$ in $J$ band (Hales et al. 2006). Unlike most Herbig Ae stars, HD 169142 was detected in the *ROSAT* All Sky Survey (RASS).[19] Adopting $d = 145$ pc (Sylvester et al. 1996), the RASS count rate of $0.06 \pm 0.02$ counts $s^{-1}$ is comparable to the RASS count rate for HD 104237 scaled to 145 pc. The identification of a young stellar association for HD 104237 in the optical (Grady et al. 2004) and X-ray (Feigelson et al. 2003) suggested that HD 169142 might also have low-mass companions.

## 2. OBSERVATIONS AND DATA REDUCTION

To further characterize the disk and to date the star, we have obtained *HST* NICMOS coronagraphic imagery, *HST* ACS FUV imagery, *Chandra* ACIS imagery, Goddard Fabry-Perot narrowband optical imagery, and classification dispersion optical spectra at the Apache Point Observatory 3.5 m telescope. These data are supplemented by archival 2MASS, *Spitzer*, and *IUE* data.

### 2.1. *NICMOS Coronagraphic Imagery*

We conducted *HST* NICMOS imaging of HD 169142 on 2005 April 30 UT with NICMOS camera 2 as part of a larger coronagraphic survey of protoplanetary and young debris disks (HST-GO-10177, G. Schneider, PI). The observations of HD 169142 were obtained at two spacecraft roll angles separated by 29.9° obtained within a single orbit (visits 33 and 34 of HST-GO-10177). Each visit consisted of F171M target acquisition imaging (ACQ), deep coronagraphic (CORON) images obtained in the F110W ($\lambda_{\rm eff} = 1.104$ $\mu$m, FWHM = 0.5915 $\mu$m) filter, and following a $2.83''$ slew, direct-light imaging of the core-saturated unocculted (DIRECT) stellar point-spread function (PSF). The pixel scale for NICMOS camera 2 is $\sim$75.8 mas $pixel^{-1}$. Calibration and data reduction followed Schneider et al. (2005). A reduced and calibrated image of the visit 33 oriented NICMOS camera 2 field, with HD 169142 centered in the coronagraphic obscuration, is shown in Figure 1*a*.

Use of the coronagraph results in a contrast gain ranging between a factor of a few to 10 within a few arcseconds of the star, compared to direct imaging (Schneider et al. 2001). The residual levels of instrumentally diffracted and scattered starlight were further reduced using two PSF subtraction techniques: "134 roll-differencing" (Lowrance et al. 1999), and template PSF subtraction. For roll-differencing, the orientation-invariant target stars' coronagraphically occulted PSF serves as its own subtraction template, revealing asymmetries in any circumstellar nebulosity (Fig. 1*b*). For template PSF subtraction (see Schneider et al. 2006), template PSFs are selected from coronagraphic images of stars with $J - H$ colors similar to those of the target, and no evidence for nebulosity on a scale larger than the NICMOS coronagraphic spot.

For all of the CORON images, the location of the star(s) occulted by the coronagraphic obscuration was determined using the spacecraft offset slew vectors downlinked in engineering

[19] See Voges et al. (1999) for the RASS Bright Source Catalogue. The RASS Faint Source Catalogue is at http://www.xray.mpe.mpg.de/rosat/survey/rass-fsc/.

TABLE 1
JOURNAL OF NICMOS OBSERVATIONS

| HD | Visit | Orientation (deg) | Type | Filter | Readout Mode | $t_{exp}$ (s) | Observation ID (N8ZU+) |
|---|---|---|---|---|---|---|---|
| 169142 | 33 | 34.0 | Acquisition | F171M | ACQ (ACCUM) | 0.46 | 33ZYQ |
| | ... | ... | Coronagraphic | F110W | STEP32/NSAMP14 | 3 × 224 | 33010, 33ZZQ |
| | ... | ... | Direct | F110W | SCAMRR/NSAMP25 | 10.15 | 33020 |
| | 34 | 63.9 | Acquisition | F171M | ACQ (ACCUM) | 0.46 | 34A7Q |
| | ... | ... | Coronagraphic | F110W | STEP32/NSAMP14 | 3 × 224 | 34010, 34AAQ |
| | ... | ... | Direct | F110W | SCAMRR/NSAMP25 | 10.15 | 34020 |
| 22128 | 41 | 166.9 | Acquisition | F171M | ACQ (ACCUM) | 0.41 | 41GIQ |
| | ... | ... | Coronagraphic | F110W | STEP32/NSAMP14 | 3 × 224 | 41010, 41GLQ |
| | ... | ... | Direct | F110W | SCAMRR/NSAMP16 | 6.50 | 41020 |
| | 42 | 195.9 | Acquisition | F171M | ACQ (ACCUM) | 0.41 | 42GP1 |
| | ... | ... | Coronagraphic | F110W | STEP32/NSAMP14 | 3 × 224 | 42010, 42GSQ |
| | ... | ... | Direct | F110W | SCAMRR/NSAMP16 | 6.50 | 42020 |
| 142666 | 2B | 44.0 | Acquisition | F171M | ACQ (ACCUM) | 0.39 | 2BEQQ |
| | ... | ... | Coronagraphic | F110W | STEP32/NSAMP14 | 3 × 224 | 2B010, 2BEUQ |
| | ... | ... | Direct | F110W | SCAMRR/NSAMP25 | 10.15 | 2B020 |
| | 2C | 73.9 | Acquisition | F171M | ACQ (ACCUM) | 0.39 | 2CEZQ |
| | ... | ... | Coronagraphic | F110W | STEP32/NSAMP14 | 3 × 224 | 2C010, 2CF2Q |
| | ... | ... | Direct | F110W | SCAMRR/NSAMP25 | 10.15 | 2C020 |
| 36112 | 31 | 196.9 | Acquisition | F171M | ACQ (ACCUM) | 0.36 | 31VNQ |
| | ... | ... | Coronagraphic | F110W | STEP32/NSAMP14 | 3 × 224 | 31010, 31VQQ |
| | ... | ... | Direct | F110W | SCAMRR/NSAMP25 | 10.15 | 31020 |
| | 32 | 226.8 | Acquisition | F171M | ACQ (ACCUM) | 0.36 | 32VZQ |
| | ... | ... | Coronagraphic | F110W | STEP32/NSAMP14 | 3 × 224 | 32010, 32W2Q |
| | ... | ... | Direct | F110W | SCAMRR/NSAMP25 | 10.15 | 32020 |
| 220750 | 73 | 329.2 | Acquisition | F171M | ACQ (ACCUM) | 0.50 | 73KAQ, |
| | ... | ... | Coronagraphic | F110W | STEP32/NSAMP14 | 3 × 224 | 73010, 73KDQ |
| | ... | ... | Direct | F110W | SCAMRR/NSAMP11 | 4.47 | 73020 |

telemetry. These offset vectors were applied to the star's position measured from the corresponding preslew ACQ image. Stellar image centroids were determined by Gaussian profile fitting using the NICMOS IDT's IDP3 software (Schneider & Stobie 2002). The calibrated HD 169142 image from visit 34, and all of the PSF template stars (see Table 1), were co-aligned to the location of HD 169142 in the visit 33 image by shifting to the location of the visit 33 image with IDP3's bicubic sinc function apodized interpolative resampling. With the two HD 169142 images translationally registered, simple image subtraction showed only symmetric PSF subtraction residuals (Fig. 1*c*) appropriate to data taken with different thermally induced *HST* focus (''breathing''). The roll-differenced data are consistent with either a nebulosity nondetection or an azimuthally symmetric disk.

The template PSF images are drawn from program stars that were at least as bright as HD 169142, and from the spectral type range B9–F2, to minimize color effects under the F110W filter. PSF template candidate stars with known thermal IR excesses were retained only after they were shown to exhibit no detectable circumstellar scattered light excesses after being subjected, themselves, to template PSF subtraction. Since the movement of the *HST* secondary mirror on 2004 December 24 produced small but measurable changes in the coronagraphic PSF, we further restricted the candidate PSF template stars to objects with data obtained after that date. Four program stars had data meeting these combined criteria (Table 1).

The flux densities of the PSF template stars were renormalized to that of HD 169142 by nulling (via iterative scaled subtraction) of the DIRECT images outside of the PSF core saturation radii. Next, we separately registered and subtracted both visits for each PSF template star from each of the HD 169142 visits, after scaling their intensities, separately, from the visit 33 and visit 34 images of HD 169142 (see Schneider et al. 2001 for details of process and error estimation). The star-minus-PSF template image sets were further culled to exclude observations that showed large *HST* breathing residuals when compared with the HD 169142 data. For visit 33, the data from visits 31, 32, 41, 42, 73, 2B, and 2C provided seven star-minus-PSF image sets meeting these criteria. For visit 34, the data from visits 31, 32, 41, 73, 2B, and 2C were used (Table 1). For each visit the PSF-subtracted images resulting from the V33 and V34 HD 169142 observations were median combined (with equal weight) as illustrated in (Figs. 1*d* and 1*e*), where they are also compared to typical PSF template minus PSF template subtractions (e.g., Fig. 1*f*). Circumstellar scattered light excesses are detected in all seven of the star-minus-PSF image sets for both visits 33 and 34.

### 2.2. *HST ACS Imagery*

HD 169142 was observed with *HST* and the Advanced Camera for Surveys (ACS) Solar-Blind Channel (SBC) with the F122M filter (nominal $\lambda_{\rm eff} = 1210$ Å, FWHM = 60 Å) on 2006 April 5 as part of HST-GO-10764 (Grady, PI). The data, with a total integration time of 1904 s, were obtained in four segments within a single spacecraft orbit (Table 2). For each segment, the field was dithered using the ACS small-box dither pattern (Gonzaga et al. 2005; with dither offsets of $\approx 0.15''$–$0.19''$) about the SBC-FIX aperture location. The data were processed using the default ACS pipeline software including geometric distortion correction and use of the multidrizzle algorithm to produce a co-added, geometric-distortion-corrected image (Gonzaga et al. 2006). In the final geometrically corrected and co-added imagery, the image scale is $0.025''$ pixel$^{-1}$.

TABLE 2
JOURNAL OF *HST* ACS OBSERVATIONS

| Star | Date | Observation ID | P.A. (deg) | $t_{exp}$ |
|---|---|---|---|---|
| HD 169142 | 2006 Apr 5 | j9jd02010, 20, 30, 40 | −88.68 | 4 × 476.0 |
| HS 2027+0651 | 2002 Jun 9 | j8c102wnq | −56.98 | 400.0 |
| | 2003 Mar 19 | j8jq01S2Q | −96.39 | 400.0 |

The effective wavelength of a particular source in the F122M filter is a strong function of the source's spectral energy distribution (SED). While the filter throughput is strongly peaked at Ly$\alpha$, the filter passband has an extended red tail resulting in 1% throughput to 1400 Å, and some sensitivity to the long-wavelength limit of the SBC at 2000 Å. For late-type stars with FUV spectra dominated by chromospheric emission, the effective wavelength is at Ly$\alpha$. However, late A and early F stars have photospheric SEDs that change in flux density by a factor of 4500 from Ly$\alpha$ to 2000 Å. As a result, in the *absence* of excess light due to accretion and stellar activity, $\lambda_{\rm eff} = 1710$ Å. The presence of enhanced, shorter wavelength emission in the F122M imagery can be inferred only via the presence of an excess signal over expectations for a photospheric SED matched to the late A star.

The ACS F122M image, after pipeline processing, has a background level of $1.77 \pm 1.55$ millicounts pixel$^{-1}$ s$^{-1}$, equivalent to $1.2 \times 10^{-13}$ ergs cm$^{-2}$ s$^{-1}$ arcsec$^{-2}$ in Ly$\alpha$. This background, in combination with the *HST* PSF, which has a bright core subtending 4 pixels and more diffuse wings, results in a point-source detection limit (5 $\sigma$ per resolution element) of $1.3 \times 10^{-15}$ ergs cm$^{-2}$ s$^{-1}$ assuming the signal is due to Ly$\alpha$. In our image, there are no diffuse features detectable at the 3 $\sigma$ level or higher, and there are only three point sources above our point-source detection limit, in addition to the recently identified optical ghost to the upper left of the brightest source in the field (Collins et al. 2007).

### 2.3. *GFP Narrowband Imagery*

HD 169142 was observed with the Goddard Fabry-Perot (GFP) Interferometer at the Apache Point Observatory 3.5 m telescope on 2005 May 5 and 2006 July 22–23 (Table 3). The GFP instrument is discussed by Gelderman et al. (1995) and more recently Wassell et al. (2006). Our observations were made with a resolution of 1200 km s$^{-1}$ for the purpose of searching for H$\alpha$ emission objects in the vicinity of HD 169142. Our data were obtained with the coronagraphic wedge in the optical path, but with HD 169142 *unocculted*. At the APO 3.5 m, the field of view of the GFP is a 1.65′ radius circle. GFP data reduction is described in Wassell et al. (2006). The seeing in the 2005 observations was 2″, while the seeing in the 2006 imagery was 1″.

### 2.4. *Optical Classification Dispersion Spectroscopy*

Optical long-slit spectroscopy was carried out with the Double Imaging Spectrograph (DIS)[20] on the ARC 3.5 m telescope at APO (Table 4). While DIS is a dual channel system, we made use of only the red channel, covering 0.55–1 $\mu$m. At the epoch of our observations, the spatial pixel scale at the detectors is 0.40″ pixel$^{-1}$. The HD 169142 observations were made with the slit oriented along P.A. = 44°. These data, from 2005 May 28 and at higher dispersion on 2005 June 30, were supplemented by spectra of K and M spectral type standard stars from Kirkpatrick et al. (1991) on 2005 June 30 (Table 4). The 2005 May 28 spectrum of HD 169142 was obtained with the Herbig Ae star occulted by a 2″ wide bar, while the 2005 June 30 data were obtained with HD 169142 unocculted. Wavelength calibration was done using a He-Ne-Ar lamp, and the spectra were extracted and background subtracted using self-developed IDL scripts. No compensation was made for the wavelength-dependent sensitivity of DIS.

### 2.5. *Chandra Observations*

HD 169142 was observed by the *Chandra X-Ray Observatory* on 2006 May 16 for 10.0 ks (sequence ID 200404 under program 7200493, Grady, PI) using the Advanced CCD Imaging Spectrometer (ACIS; Garmire et al. 2003). To ensure the highest soft energy response, HD 169142 was placed at the ACIS-S aim point, and data were obtained using the default 8.3′ × 50.6′ field of view. When used as an imager in this configuration, ACIS-S provides imagery with a FWHM = 0.5″ and pulse-height spectra from 0.3 to 8.0 keV.

For the analysis, we used the CIAO[21] software package, version 3.3 (CALDB ver. 3.2.2). Within 30″ of the aim point, *Chandra* detected two sources, confirming the *ROSAT* detection as indicating the presence of more than one X-ray source. One, located at (R.A., decl.) = (276.124, −29.780) (J2000.0), corresponding to $18^{\rm h}24^{\rm m}29.79^{\rm s}$ and $-29°46'49.7''$, was 0.3″ from the nominal position of HD 169142, well within the 90%

[20] The Double Imaging Spectrograph was built at Princeton University by J. Gunn, M. Carr, B. Elms, R. Lucinio, R. Lupton, and G. Pauls. See http://www.apo.nmsu.edu/35m_operations/35m_manual/Instruments/DIS/DIS_quick_info.html.

[21] See http://cxc.harvard.edu/ciao/.

TABLE 3
JOURNAL OF GFP OBSERVATIONS

| Date | Etalon | $R$ (km s$^{-1}$) | Filter | Width (Å) | Line | $t_{exp}$ (s) | Comments |
|---|---|---|---|---|---|---|---|
| 2005 May 5 | Visible-broad | 1500 | 6563 | 120 | H$\alpha$ | 15 | On-line |
| | | | | | 6548 | 30 | Off-band |
| 2006 Jul 23 | Far-red | 1200 | 6563 | 79 | H$\alpha$ | 10 | On-line |
| | | | | | 6599 | 30 | Off-band |

TABLE 4
Journal of DIS Optical Spectra

| Star | Spectral Type | Date | Resolution | Slit (arcsec) | $\lambda_{cen}$ | $\lambda$ (Range) | $t_{exp}$ (s) | P.A. Slit |
|---|---|---|---|---|---|---|---|---|
| HD 169142 | A8 Ve | 2005 May 28 | 1500 | 1.2 | 7500 | 4500 | 600 | 46 |
| | | 2005 Jun 30 | 4550 | 1.5 | 7300 | 1700 | 300 | 46 |
| HD 190007 | K5 V | 2005 Jun 30 | 1500 | 1.5 | 7592 | 4500 | 20 | 90 |
| GL 786 | K7 V | 2005 Jun 30 | 1500 | 1.5 | 7592 | 4500 | 85 | 90 |
| GL 763 | M0 V | 2005 Jun 30 | 1500 | 1.5 | 7592 | 4500 | 120 | 90 |
| GL 806 | M2 V | 2005 Jun 30 | 1500 | 1.5 | 7592 | 4500 | 200 | 90 |
| Barnard's star | M4 V | 2005 Jun 30 | 1500 | 1.5 | 7592 | 4500 | 100 | 90 |

uncertainty circle of *Chandra* absolution positional accuracy of $0.6''$.[22] We identify this source as HD 169142. The other source was located at $18^h24^m29.29^s$ and $-29^\circ46'56.3''$, and is further discussed in § 3.3 below. X-ray events were extracted within $2''$ of the peak for both sources, including more than 95% of the total point-source flux. We did not subtract the background, which was negligible (<1% of the source count). We generated response matrices and auxiliary files using `acisspec`.

### 2.6. *Assembling the IR SED*

The infrared data consisted of *JHK*-band observations from the 2MASS database, PHT40 observations from the *Infrared Space Observatory* (*ISO*) archives (see Acke & van den Ancker 2004), *IRAS* Faint Source Catalog photometry at 12, 25, 60, and 100 $\mu$m, and spectra observed with the Infrared Spectrograph (IRS; Houck et al. 2004) of the *Spitzer Space Telescope* (Werner et al. 2006) and obtained from the *Spitzer* data archive.

The IRS observations were originally obtained using spectral map mode as part of *Spitzer* Cycle 1 IRS GTO time, with the IRS Short-Low (SL) data discussed by Sloan et al. (2005). We used the SSC pipeline-processed, postbasic calibrated data ("pbcd") products that were processed using the C13.0PRE25A calibration. We removed all pixels flagged as questionable and extracted the spectrum using a full slit width to avoid loss of signal in the slightly spatially extended spectrum. For SL2 (5.2–8.8 $\mu$m) and SL1 (7.4–14.5 $\mu$m) we used only the scan positions with the highest signal, centered on the star. For SL2 the absolute flux levels of all the selected scans were within 5% of one another, and the weaker spectrum was scaled to match that of the stronger one, and then averaged. The strongest SL1 spectra were rescaled by 11%–15% to match the SL2 data, and merged.

The strongest Short-High (SH; 9.9–19.6 $\mu$m) echelle spectra were extracted in a similar fashion, and scaled upward by 15% to match the longest wavelength SL1 data. The overlap among the orders was good, and no rescaling of individual spectral orders was done. The Long-High (LH; 18.7–37.2 $\mu$m) spectra were of lower quality. The most heavily exposed data suffered from significant mismatch between orders, and were close to saturation at the longest wavelengths. Those with slightly lower signals had better order-to-order consistency shortward of 25 $\mu$m and were selected for use. These were averaged and required a downward scaling of 15% to match as closely as possible both the SH spectra and the 25 $\mu$m *IRAS* photometry. For $\lambda \geq 27$ $\mu$m the order-to-order overlap in the flux-calibrated data was poor, and no attempt was made to rectify these data, so they must be considered of lower overall quality. No *Spitzer* data at $\lambda \geq 35.4$ $\mu$m were used. We have also made use of 0.8, 1.1, 1.3, and 2.0 mm data from Sylvester et al. (1996).

[22] See http://cxc.harvard.edu/cal/ASPECT/celmon/.

## 3. RESULTS

### 3.1. *The Disk of HD 169142 in Scattered Light*

After PSF template subtraction, circumstellar light is seen in both NICMOS coronagraphic images. The nebulosity is azimuthally symmetric, except for the effect of known PSF subtraction residuals, in agreement with the null detection of nebulosity in the roll-differenced data (Fig. 1*b*). Azimuthally symmetric nebulosity is also consistent with disk inclinations $\leq 20^\circ$ from face-on, in good agreement with the CO emission profiles (Raman et al. 2006; Dent et al. 2005), the polarimetric imaging of the disk (Hales et al. 2006; Kuhn et al. 2001), and the single H$\alpha$ emission component noted by Dunkin et al. (1997b). We trace the disk in the data for both visits in the range $0.57'' \leq r \leq 1.4''$, in agreement with the differential polarimetric imaging. Adopting $d = 145$ pc, this corresponds to a disk detection in the range 80 AU $\leq r \leq$ 200 AU (for a face-on disk). The presence of background stars at $r = 2.1''$ at three different position angles from HD 169142 in the NICMOS images places a firm upper limit on the disk radius of 300 AU at $d = 145$ pc (Fig. 1*c*). The NIR scattered light disk is in good agreement with the CO disk reported by Raman et al. (2006; Fig. 2).

We find no evidence for azimuthally differentiated scattered-light structures intrinsic to the disk, down to the detection limit imposed by imperfect PSF subtractions. Moreover, the azimuthally medianed radial surface brightness profiles for both visits can be fit by single power laws (Fig. 3). However, we consider the fit for the first visit more robust as the *HST* PSF was more stable and better matched to our reference PSFs. From those data, we find a peak surface brightness at $r = 0.57''$ of $5 \pm 1.4$ mJy arcsec$^{-2}$, with the radial surface brightness $S \propto r^{-3.0\pm0.1}$ in the range $0.57'' < r < 1.3''$. The surface brightness at $0.57''$ is comparable to that of TW Hya (Weinberger et al. 2002), *without compensation for the greater distance to HD 169142*. However, the surface brightness drops at a rate that is steeper than for TW Hya, but comparable to HD 100546 (Grady et al. 2001; Augereau et al. 2001), and is only slightly less steep than seen in $\beta$ Pic beyond 100 AU (Golimowski et al. 1993). After correction for the $r^{-2}$ falloff in the stellar radiation field, we find that the surface density of scatterers in the HD 169142 disk is $\propto r^{-1}$.

### 3.2. *Near-IR Imagery of the Field*

With $l = 3.39^\circ$ and $b = -7.81^\circ$, HD 169142 is viewed against the Galactic bulge, with numerous faint stars visible in the relatively small $19.2'' \times 19.3''$ field of view of the NICMOS detector. The brightest object in the field, apart from the occulted HD 169142, is a source $9.3''$ from HD 169142 to the southwest

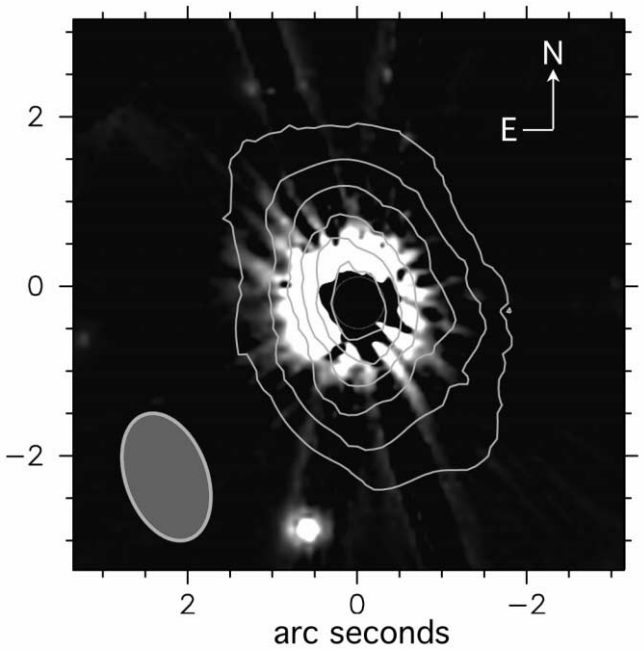


FIG. 2.—Comparison of the F110W scattered-light image with the continuum contours from Raman et al. (2006). The NICMOS image combines the PSF-subtracted frames from both visits (rotated to a common celestial orientation and averaged) with the same linear stretch as seen in Fig. 1. The contours show CO($J = 2$–1) emission at 230 GHz imaged by the SMA (see Raman et al. 2006 for details). The beam size is $1.6'' \times 1.0''$, P.A. 20°. The contour increment is 0.4 Jy km s$^{-1}$. The apparent ellipticity of the CO emission from the disk results from the interferometer geometry coupled with the southern declination of the star (Raman et al. 2006). The SMA contours were registered on the position of the star occulted by the $0.3''$ radius NICMOS coronagraph (represented by the white circle).

of the star (Fig. 1*a*). This source is marginally resolved from HD 169142 in 2MASS imagery (Fig. 4*a*) and is cataloged as 2MASS 18242929−2946559 (hereafter 2M1824) with $J = 9.894 \pm 0.032$, $H = 9.265 \pm 0.031$, and $K = 9.024 \pm 0.030$. The $J - K$ color is $0.874 \pm 0.044$, typical of unreddened late-type stars lacking near-IR excess light. Closer inspection of 2M1824 in the NICMOS F110W data (Fig. 5) shows that it is resolved in both visits into two sources separated by $130 \pm 20$ mas. The F110W band flux densities of the two components of the 2M1824 system were determined by iteratively simultaneously subtracting Tiny Tim (noiseless) model PSFs (for spectral class M2 sources, so well color matched), with $\chi^2$ minimization in the difference image, treating the star positions and intensity scaling as free parameters. We find $\Delta J \approx 0.19$ for the components, adopting spectral types of M2 V and using the STSDAS `calcphot` task (Table 5). Following PSF subtraction, an additional object is marginally detected with F110W magnitude comparable to the other faint objects in the field.

### 3.3. *Nearby T Tauri Stars*

M stars that are coeval with a Herbig Ae star should still be in the T Tauri phase and exhibit net H$\alpha$ emission, conspicuous X-ray emission, and if unreddened, Ly$\alpha$ emission. Subtraction of the off-band imagery from the GFP H$\alpha$ data demonstrates that both HD 169142 and 2M1824AB have net H$\alpha$ emission, together with the expected factor of 100 intensity ratio appropriate for a Herbig Ae star and any associated late K to early M T Tauri companion (Figs. 4*b*–4*d*). The initial DIS spectrum of both stars confirmed the presence of H$\alpha$ emission in HD 169142 and 2M1824AB. The higher resolution 2005 June 30 spectrum of HD 169142 shows the partial filling in of H$\alpha$ and an emission profile similar to that reported at higher dispersion by Dunkin et al. (1997b). The blended 2M1824AB spectrum is cleanly separated from HD 169142 at both epochs. H$\alpha$ emission

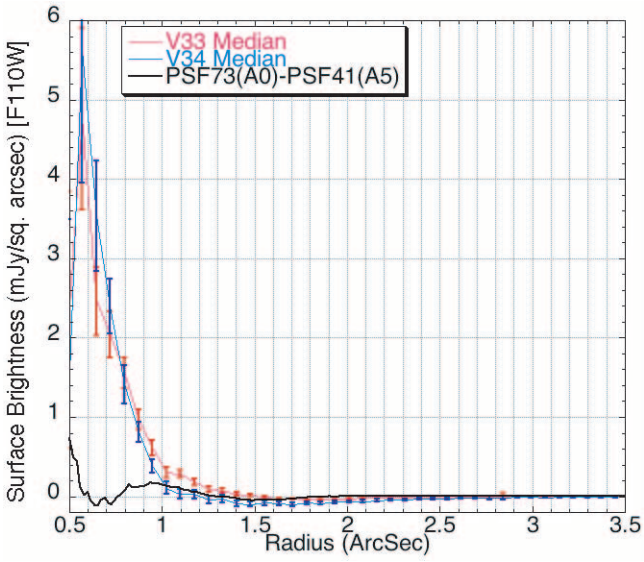


FIG. 3*a*

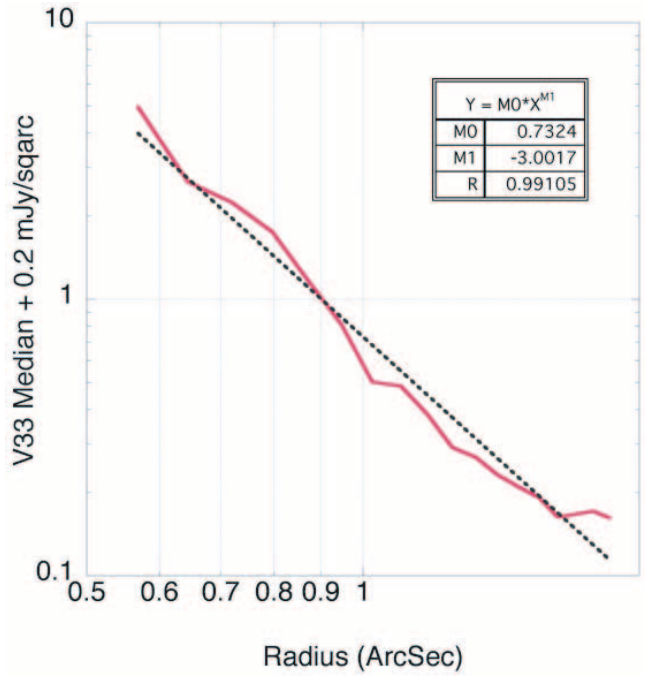


FIG. 3*b*

FIG. 3.—(*a*) Azimuthally medianed radial surface brightness profiles for V33 and V34, together with azimuthally averaged PSF − PSF data. (*b*) The V33 data can be fit by $r^{-3.0 \pm 0.1}$ from $0.57''$ to $1.3''$.

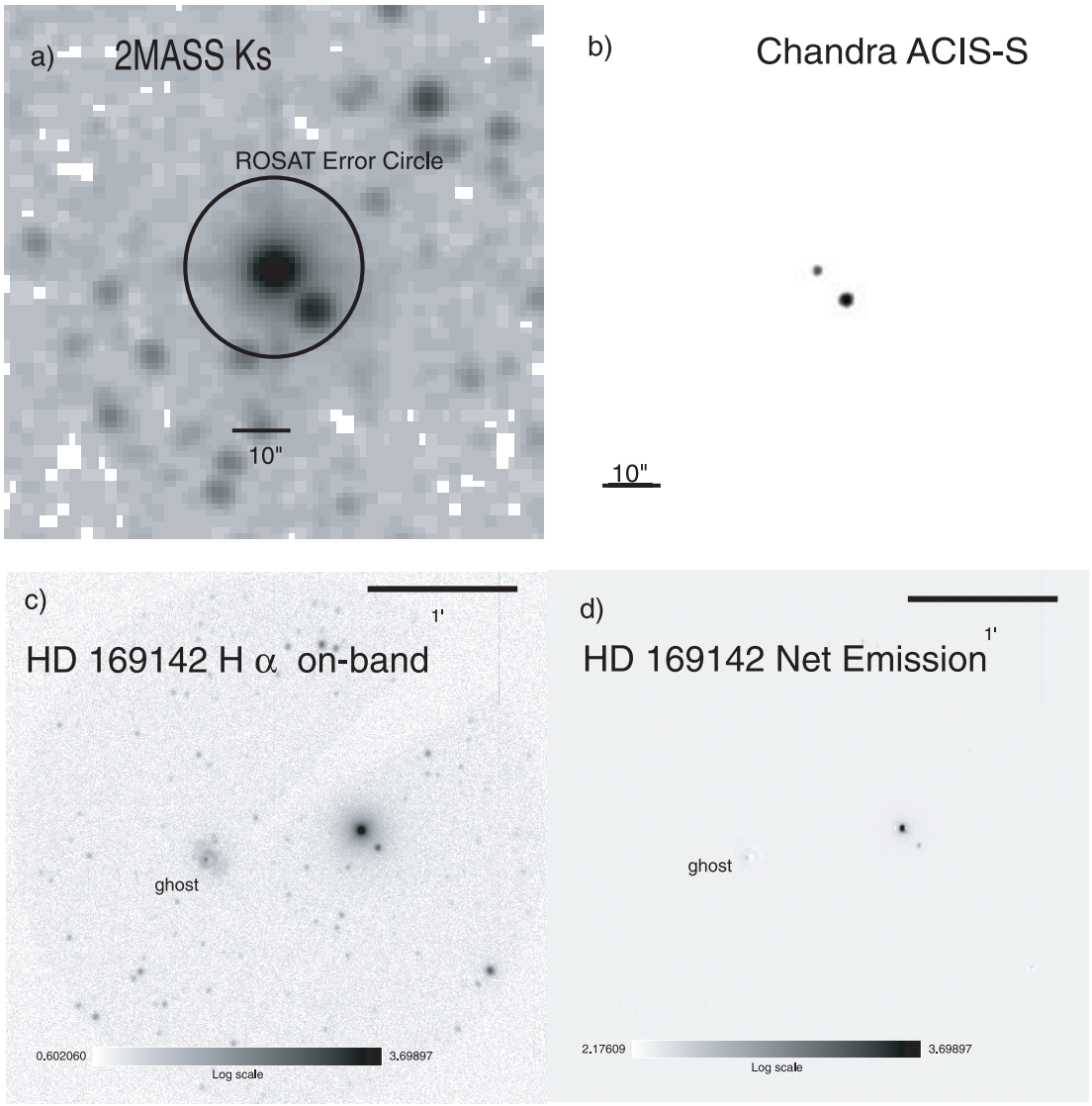


FIG. 4.—Environment of HD 169142. (*a*) 2MASS $K_s$ imagery showing both HD 169142 and 2M1824. The RASS error circle for HD 169142 is shown superposed on the 2MASS data. Both stars fall within the RASS error circle. (*b*) A portion of the *Chandra* ACIS data at the same spatial scale as the 2MASS data. The only sources visible are HD 169142 and 2M18424. (*c*) Optical ultranarrowband imagery at H$\alpha$ (*c*) prior to and (*d*) following subtraction of an off-band image. The only sources in the net image are HD 169142 and 2M1824. All data are shown with north up and east to the left.

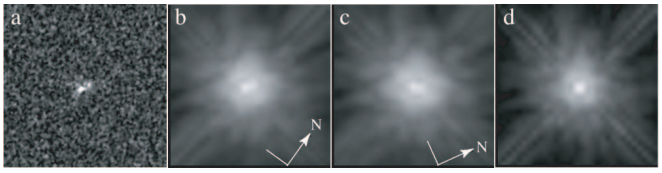


FIG. 5.—Individual components of the 2M1824 binary system, separated by 0.13″, are seen in the ACS UV and NICMOS near-IR imagery. The stars are cleanly separated in the ACS image (panel *a*; linear 8 bit display from −0.003 to +0.013 counts $s^{-1}$ $pixel^{-1}$), thanks to the order-of-magnitude superior spatial resolution achieved at 0.122 $\mu$m compared to the NICMOS 1.1–1.7 $\mu$m filter bands employed, but are of marginal S/N in the UV due to the redness of the M star components. The ACS image is shown at the same image orientation as the first of the two NICMOS frames (*b*, *c*). The binary is well exposed in the fields of these deep NICMOS F110W coronagraphic images and the relative positions of the components exactly track the 29.9° change in celestial orientation of the field relative to the frame of the detector fixed to the spacecraft. The NICMOS images are shown with a $\log_{10}$ display stretch from [0] to [4.5] dex counts per second per pixel to illustrate the rotation of the binary orientation with the spacecraft against the (much fainter) "fixed" pattern of the spatially extended wings of the stellar PSFs. For comparison, a similarly observed single-star PSF is shown (*d*) scaled to the F110W flux density of 2M1824.

is present in the 2005 and 2006 spectra with the same equivalent width, consistent with either the more luminous or both of the stars in 2M1824AB being weak-line T Tauri stars. When compared with the Kirkpatrick et al. (1991) spectral standards, we find an aggregate spectral type of M2.5 Ve (Fig. 6).

In total,*Chandra* detected ≈660 photons at the position of 2M1824AB in the 10 ks integration, with the two stars blended into a single X-ray source. There were sufficient counts in this composite source to fit a two-temperature component + absorption model to the pulse-height spectrum (Fig. 7). We find $kT_1 = 1.5$ keV, while $kT_2 = 0.46$ keV, with $Z \approx 0.29$ solar and $N(\mathrm{H}) = 3.6 \times 10^{20}$ $cm^{-2}$. The observed flux from 0.3 to 2 keV is $F_X = 2.1 \times 10^{-13}$ ergs $cm^{-2}$ $s^{-1}$. For the 2M1824AB components, $L_X$ is typical of weak-lined T Tauri stars, as is the combined pulse-height spectrum.

Raman et al. (2006) included 2M1824AB in their HD 169142 observations, but did not detect the binary in either the millimeter continuum or CO, suggesting that the individual components in 2M1824AB lack cold disk material. This behavior is similar to HR 4796B, and HD 141569B and HD 141569C.

TABLE 5
2MASS 18242929−2946559

| Star | F110W Magnitude | *J* |
|---|---|---|
| 2MASS 18242929−2946559A ..... | 11.35 ± 0.17 (0.051 Jy) | 11.02 ± 0.18 |
| 2MASS 18242929−2946559B..... | 11.54 ± 0.20 (0.043 Jy) | 11.21 ± 0.21 |

### 3.4. *Proper Motion*

The physical association of HD 169142 with 2M1824AB can be tested through differential proper motion measurements. HD 169142's proper motion as given in the SIMBAD database is $\mu_\alpha = -4.7 \pm 4.1$ mas yr$^{-1}$, $\mu_\delta = -43.1 \pm 3.6$ mas yr$^{-1}$. For NICMOS we used the two critically sampled F171M target acquisition images to directly establish the position of HD169142 (obscured in our deep coronagraphic imagery) with 2D Gaussian profile fitting. Two-component PSF fitting, using Tiny Tim version 6.3 (noiseless) model PSFs, was employed to determine the positions of the A/B components of 2M1824 due to the partial overlap of the component PSFs. All three sources were individually well resolved in the ACS image and amenable to direct image centroid determination. The relative positions of all three components could be measured with high precision, separately, in the ACS and NICMOS frames. However, a small (but undetermined) systematic error in the orientation of the ACS aperture in the celestial frame, coupled with the less than 1 yr baseline between the ACS and NICMOS observational epochs, did not permit a statistically significant measurement using this pair of images.

We therefore used an earlier epoch (1998 July 19) 2MASS *H*-band image (resampled 1″ pixel$^{-1}$ scale) to measure, and establish, the two-epoch relative proper motions. At the image scale and sampling of the 2MASS image, the A/B components of 2M1824 were unresolved (fully blended), hence an A/B image centroid yields a photocentric position. We therefore remeasured a combined A/B position from the NICMOS images using an aperture-enclosing weighted-moment measure. We chose the 2MASS *H*-band image since the NICMOS F171M bandpass is fully contained within 2MASS *H*, thus minimizing a potential photocentric displacement with wavelength due to the individual SEDs of the A/B stars.

Thus, we establish a relative proper motion of $\Delta\mu_\alpha = 16.7 \pm 12.8$ mas yr$^{-1}$ and $\Delta\mu_\delta = 3.0 \pm 9.7$ mas yr$^{-1}$. If 2M1824AB were a background object, we would have expected $\Delta\mu_\alpha = -4.7 \pm 4.1$ mas yr$^{-1}$ and $\Delta\mu_\delta = -43.1 \pm 3.6$ mas yr$^{-1}$. Thus we establish a 4 $\sigma$ likelihood of common proper motion based on the expected reflective $\Delta\mu_\delta$ motion (i.e., $-292 \pm 24$ mas over the 6.78 yr baseline, whereas only $-20 \pm 66$ mas is measured over that interval). We note that our differential measures of $\Delta\mu_\alpha$ are not quite as well determined, and we measure $-113 \pm 87$ mas of relative motion over that time interval, whereas $-32 \pm 28$ mas is expected. This is statistically different from $\Delta\mu_\alpha = 0$, but only by 1.3 $\sigma$, suggesting the 2MASS measurement errors may be marginally underestimated.

### 3.5. *Exclusion of Foreground M Stars*

Foreground M stars with magnitudes similar to 2M1824AB are located at $d \leq 30$ pc and have proper motions $\geq$50 mas yr$^{-1}$. Most importantly, such objects are sufficiently X-ray bright that they are RASS sources with count rates $\geq$1 count s$^{-1}$, 16 times above the combined *ROSAT* count rate for the system. The X-ray data thus firmly exclude a chance coincidence with foreground M stars, *independently* of the proper-motion data.

### 3.6. *Exclusion of Background Stars*

The NICMOS imagery shows hundreds of faint stars, as well as HD 169142 and 2M1824AB. In contrast, Ly$\alpha$ imagery will detect only objects with both low foreground selective extinction and H I columns. In marked contrast to the NICMOS F110W imagery, the ACS F122M image is sparse, with only HD 169142 and 2M1824AB detected (peak pixel S/N of 5 and 3 for components A and B, respectively; Fig. 8). The F122M data provide no indication of the presence of the putative third component to 2M1824AB, suggesting that it is a background star. The combination of low relative proper motion, the X-ray data, and the low foreground extinction toward HD 169142 and 2M1824AB suggests that all three objects must lie at essentially the same distance. The presence of three pre–main-sequence (PMS) stars with a projected separation of 1160 AU at $d = 145$ pc is consistent with the stars being members of an aggregate similar to that associated with HD 104237 (Grady et al. 2004) or HD 141569A (Weinberger et al. 2000).

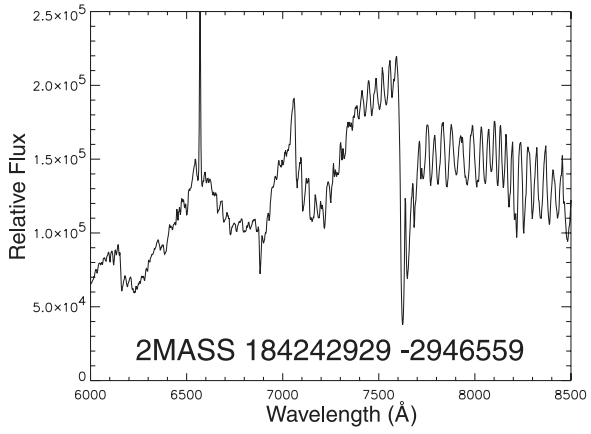


FIG. 6*a*

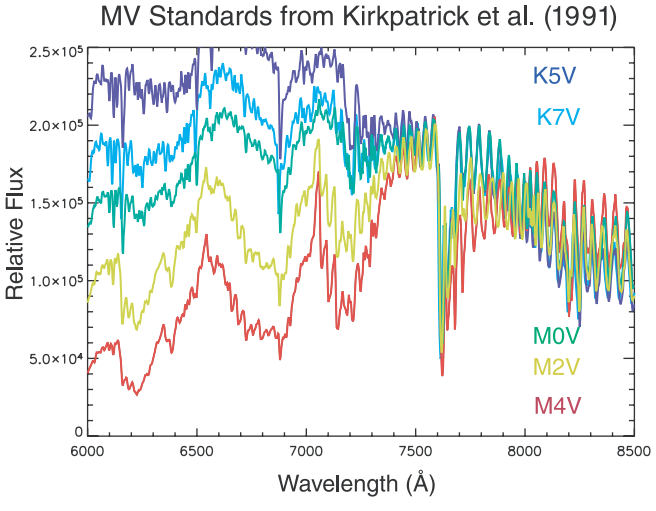


FIG. 6*b*

FIG. 6.—Spectral type of 2M1824. (*a*) The $R = 4550$ spectrum of 2M1824 from 2005 June 30. (*b*) Grid of M spectral standard stars, HD 190007 (K5 V), GL 786 (K7 V), GL 763 (M0 V), GL 806 (M2 V), and Barnard's star (M4 V). Using the spectral types assigned by Kirkpatrick et al. (1991), these standard stars bracket 2M1824AB and indicate a type of M2.5 Ve. We assign this spectral type to the brighter of the two stars.

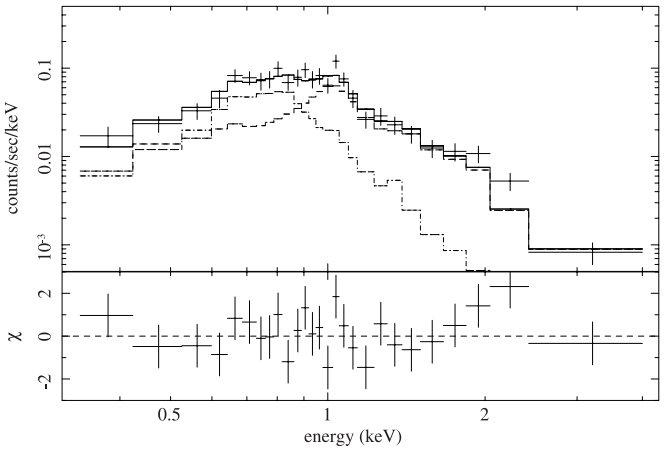


FIG. 7.—Pulse-height spectrum of 2M1824 is typical of weak-line T Tauri stars. The individual thermal components are shown as dashed histograms, while the two-temperature model ($kT_1 = 1.5$ keV, $kT_2 = 0.46$ keV, with $N_H = 3.6 \times 10^{20}$ cm$^{-2}$) is shown as a solid histogram. Residuals to the fit are shown below.

### 3.7. *Dating 2M1824AB*

*J* magnitudes derived from the NICMOS F110W data (Table 5), assuming a type of M2 V, are consistent with both stars being T Tauri stars located at $d = 145$ pc, the inferred distance for HD 169142 (Sylvester et al. 1996). We find $M_J = 5.21$ and $5.40 \pm 0.20$ for each star. Following Weinberger et al. (2000) and using the evolutionary tracks of Barraffe et al. (1998), we derive an age of $6^{+6}_{-3}$ Myr, with errors dominated by the distance uncertainties for HD 169142 (Fig. 9). 2M1824A lies on the 0.35 $M_\odot$ evolutionary track, while 2M1824B should be an $\approx$0.3 $M_\odot$ star. Thus, HD 169142 is roughly coeval with HR 4796A and the members of the TW Hydrae association and slightly younger than the $\beta$ Pictoris moving group (BPMG).

### 3.8. *HD 169142 as a Star*

In the optical, HD 169142 has the spectrum of an A5 V star (Dunkin et al. 1997a) with H$\alpha$ emission partially filling in the photospheric absorption profile and some weakness in absorption profiles, which suggests that the star might be chemically peculiar. With $(B - V) = 0.31$ and a type of A5 V, the star should be reddened by 0.14. Inspection of the spatially resolved spectral image for IUE SWP 55483[23] reveals circumstellar Ly$\alpha$ emission superposed on the image of the *IUE* large aperture in the light of the geocorona. Detection of such emission indicates $E(B - V) \leq 0.08$ mag for selective extinction by the diffuse ISM (Roberge et al. 2001). With $v \sin i = 55 \pm 2$ km s$^{-1}$ (Dunkin et al. 1997a, 1997b), HD 169142 was initially interpreted as a slow rotator, making any chemical peculiarity understandable. However, combining the system inclination $i = 13°$ (Raman et al. 2006) with the $v \sin i$ data suggests that far from being a slow rotator, HD 169142 has $v_{eq} = 240$ km s$^{-1}$, similar to that of Altair ($v_{eq} = 245$ km s$^{-1}$). Chemical peculiarities, while common in slowly rotating A stars, are unexpected in rapid rotators, unless the parent molecular cloud differed significantly from solar composition. Collectively, these data suggest that we need to revisit the spectral type identification, the inferred selective extinction toward this star, and the identification of the star as chemically peculiar.

The *IUE* SWP spectrum of HD 169142 has too little flux at $\lambda \leq 1800$ Å compared to A5 V standard stars, but is intermediate between Altair (A7 V) and HD 27176 (A8 V; Fig. 10*a*). Overall the agreement is better with Altair than with the A8 V standard. A large latitudinal temperature gradient has been invoked to account for the angular size measurements for both Altair (Peterson et al. 2006a) and Vega (Aufdenberg et al. 2006; Peterson et al. 2006b), and has been shown to produce significant gravity darkening for Altair (Domiciano et al. 2005). With a similarly high $v_{eq}$, HD 169142 would be expected to also have

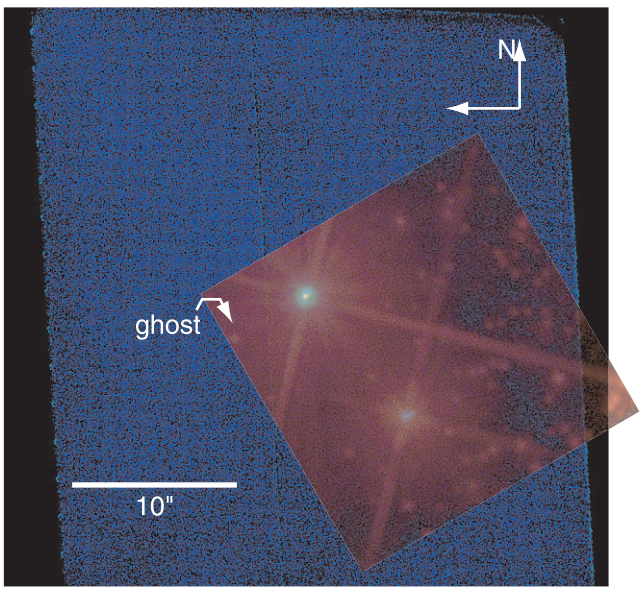


FIG. 8.—Three sources in common between the NICMOS F110W image (*red*) and the ACS SBC F122M data (*blue*) are HD 169142 and 2M1824AB shown with north up and east to the left. The UV-only feature to the southeast of HD 169142 is the identified ghost.

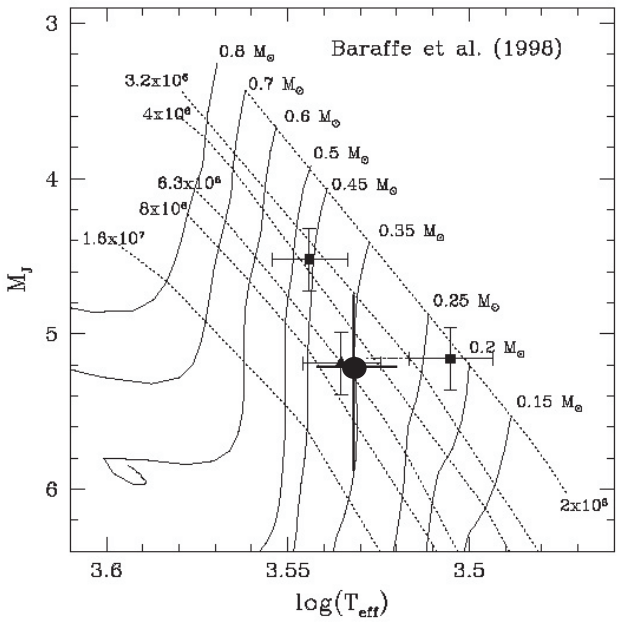


FIG. 9.—Combining the *J* magnitudes inferred from the NICMOS data with the optical spectral type allows us to place 2M1824 in the H-R diagram (*large filled circle*), along with the Baraffe et al. (1998) isochrones (after Weinberger et al. 2000). The more luminous star in the pair is essentially coeval with HR 4796B (*triangle*) and older than the companions to HD 141569 (*squares*), in good agreement with the identification of HD 169142 as a Herbig Ae star.

[23] See http://archive.stsci.edu/cgi-bin/iuebrowse?camim=swpa55483&filetype=si.

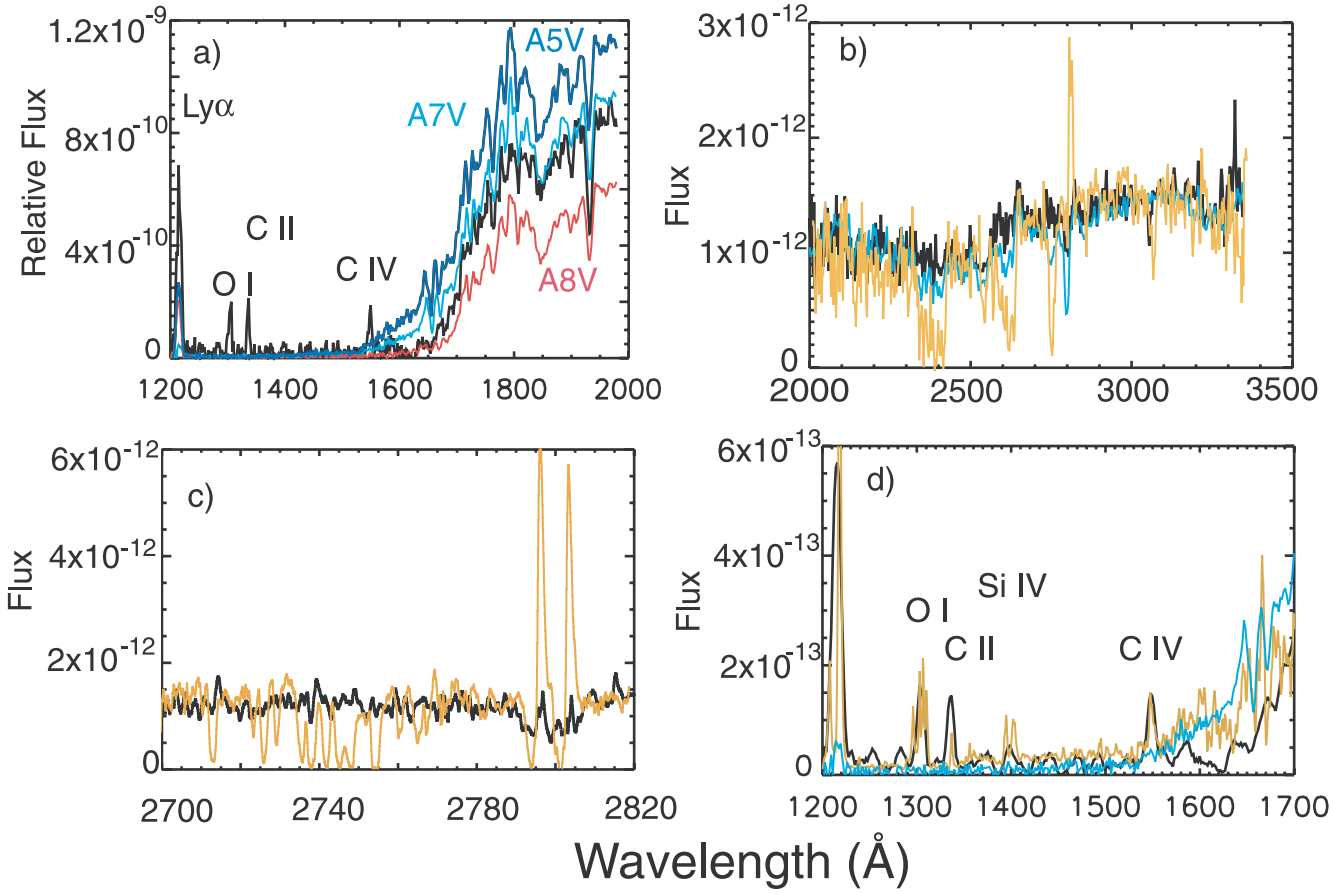


FIG. 10.—HD 169142 in the UV (*black*). (*a*) HD 169142 (IUE SWP 55483) and UV spectral type standards: A5 V (80 UMa, IUE SWP 10283; *navy*), A7 V (Altair, IUE SWP 45755; *sky blue*), A8 V (HD 27176, IUE SWP 27176; *red*), with all stars scaled to $V = 0.88$. (*b*) HD 169142 (IUE LWP 31285) compared with Altair (IUE LWP 26232) and HD 104237 (IUE LWP 32306; *orange*), with the comparisons scaled to $V = 8.15$. (*c*) The region around Mg II for HD 169142 (IUE LWP 30558) compared with a representative spectrum of HD 104237 (IUE LWP 25939). (*d*) IUE FUV spectrum of HD 169142 (IUE SWP 55483) compared with Altair (IUE SWP 45755) and HD 104237 (*HST* STIS ID = o6bt01030). HD 169142 lacks the UV excess seen in HD 104237.

significant gravity darkening, producing UV spectra that appear later than the inferred optical spectral type. The trend of later UV type in HD 169142 suggests that the star also has a significant pole-to-equator temperature gradient, which could be verified using the current generation of interferometers. Both Vega and HD 169142 have anomalously underabundant Mg in their optical spectra (Dunkin et al. 1997a, 1997b), and both are viewed pole-on, with the hot polar cap facing toward us. This suggests that temperature effects rather than chemical composition anomalies might be responsible for the absorption line peculiarities. While HD 169142 has been claimed as a Vega-like star since the discovery of its IR excess (Walker & Wolstencroft 1988), the combination of a face-on disk and a rapidly rotating star suggests that this system truly offers a view of a younger Vega.

### 3.9. *UV Limits on Accretion and Mass Loss*

A distinctive feature of the mid-IR SED of HD 169142 is the deficit of excess thermal emission shortward of 20 $\mu$m compared to the majority of Herbig Ae stars (Sylvester et al. 1996; Meeus et al. 2001; van Boekel et al. 2003; Sloan et al. 2005). Such an SED can be produced by geometric shadowing of the inner few AU of the disk by material at the dust sublimation radius (Dullemond & Dominik 2004a, 2004b), grain growth beyond the size where a significant thermal signature is expected (opacity effect), or mechanisms such as photoevaporation or dynamical sculpting that would remove material from the inner disk. The IR data for HD 169142 are ambiguous as to how much material is in the inner disk: the absence of the 10 $\mu$m silicate emission can be due either to grain growth beyond 3 $\mu$m (Dent et al. 2006) or to an absence of silicates in the inner disk. The mid-IR spectrum of HD 169142 is rich in PAH features, which have recently been spatially resolved (Habart et al. 2006). The radial SB profile rolls over in the PAH transitions at $r \leq 20$ AU. In the absence of shadowing, such a profile requires that the PAH molecules are underabundant in the inner disk, compared to the outer disk: distributions that are constant with radius would produce emission that is very strongly peaked on the star, given the $r^{-2}$ falloff in the stellar radiation field. Alternatively, the PAH data may indicate a partially evacuated cavity with $r \approx 20$ AU.

Accretion onto PMS stars produces not only enhanced emission in transitions otherwise associated with chromospheres and transition regions, but also an enhanced UV continuum flux that can be detected against the light of a late A star shortward of 2000 Å and jets that can be imaged in Ly$\alpha$ (Calvet et al. 2004; Grady et al. 2004). FUV flux excesses, enhanced emission lines in species commonly associated with chromospheric and transition region temperature plasma, and the presence of jets and/or Herbig-Haro (HH) knots are seen both for Meeus group I objects such as AB Aur (Endres et al. 2005) and for Meeus group II disks such as HD 163296 (Devine et al. 2000), HD 104237 (Grady et al. 2004), and MWC 480 (Stecklum et al. 2007). When viewed at low inclination, as for AB Aur or HD 104237, these systems exhibit type I P Cygni profiles in Mg II (Grady et al. 1996;

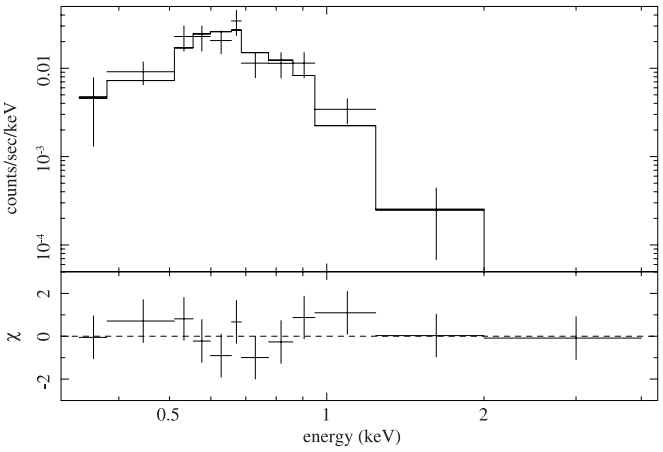


FIG. 11*a*

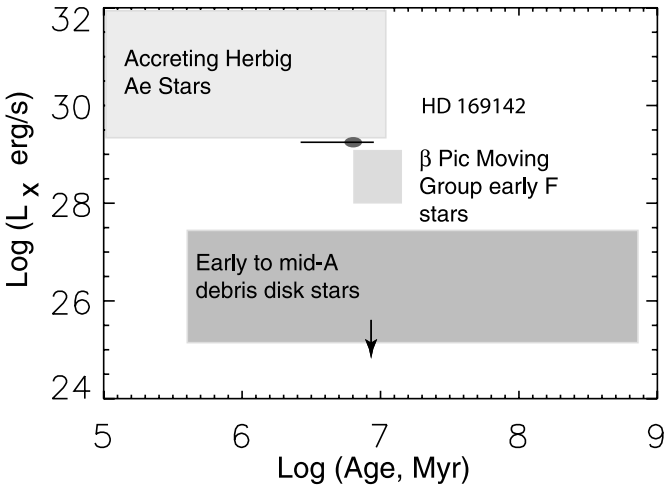


FIG. 11*b*

FIG. 11.—(*a*) Pulse-height spectrum of HD 169142, together with the single-temperature model with residuals to the model fit below. The pulse-height spectrum is soft, similar to 51 Eri (Feigelson et al. 2006) and typical of X-ray production in winds. (*b*) $L_X$ for HD 169142 is intermediate between the actively accreting Herbig Ae stars, which have $L_X \geq 10^{29}$ ergs s$^{-1}$, and nonaccreting debris disks (*open symbols and colored boxes*). The ratio $L_X/L_{bol}$ is typical of BPMG early F stars.

Fig. 10*c*) and strong, blueshifted absorption in numerous transitions of Fe II, Mn II, and Mg I, as well as conspicuous emission in Ly$\alpha$. When compared with HD 104237, HD 169142 is conspicuous by the weakness of both the Fe II absorption and Mg II emission (Figs. 10*b*–10*d*).

When the UV spectrum of HD 169142 is compared to HD 104237, another late Herbig Ae star viewed essentially pole-on, which drives a jet (Grady et al. 2004), there is a marked flux deficit shortward of 1800 Å (Figs. 10*a* and 10*d*). We can place limits on the UV continuum excess and thus the accretion luminosity by binning the *IUE* spectrum from 1284 to 1653 Å, shortward of the photospheric Si I absorption edge. This wavelength interval includes a photospheric component as well as any chromospheric or transition region emission features, but if normalized to the photospheric spectrum can be used to crudely approximate the accretion luminosity. We find that the *IUE* FUV excess light for HD 169142 is at most a factor of 0.02–0.05 that of HD 104237, with the range dominated by the observed excess light variability of HD 104237 (Grady et al. 2004). The *IUE* data imply an accretion rate $\dot{M}_{acc} \leq (0.7\text{–}1.8) \times 10^{-9} \leq (0.7\text{–}1.8) \times 10^{-9}\ M_\odot\ \mathrm{yr}^{-1}$ in the 1990s.

We can also estimate $\dot{M}_{loss}$ by using the fact that HH knots are Ly$\alpha$ bright (Grady et al. 2004; Devine et al. 2000) for low-extinction lines of sight. The HD 163296 HH knots individually have $F_{Ly\alpha} = (5\text{–}7) \times 10^{-14}$ ergs cm$^{-2}$ s$^{-1}$ (Devine et al. 2000) for an outflow at $10^{-8}\ M_\odot\ \mathrm{yr}^{-1}$ (Wassell et al. 2006). If observed with ACS, these would produce ≈4.5 counts s$^{-1}$. No HH knots are detected in the HD 169142 Ly$\alpha$ image above sky background, implying an upper limit for flux from any HH knot that is ≈200 times less than that of the HD 163296 knots. After correcting for the larger distance to HD 169142, any HH knots associated with HD 169142 must be ≈140 times less luminous. Assuming that the emission is optically thin, $\dot{M}_{loss} \leq 7 \times 10^{-11}\ M_\odot\ \mathrm{yr}^{-1}$. This implies that $\dot{M}_{acc} \leq 7 \times 10^{-10}\ M_\odot\ \mathrm{yr}^{-1}$, assuming the 10% outflow to accretion rate scale factor typical of PMS stars (Hartmann 2005). This limit is comparable to that of TW Hya and is significantly below the level suggested by the SED modeling (Dent et al. 2006) or by Garcia Lopez et al. (2006). The UV data indicate that HD 169142 lacks the accretion rate expected for a 0.02 $M_\odot$ gas-rich disk that is coupled to the star.

### 3.10. *X-Ray Limits on Mass Loss and Accretion*

In the *Chandra* image, ≈100 photons were detected at the position of HD 169142 between 0.3 and 8 keV. The count rate for the source showed only a ∼50% increase over the course of the 10 ks observation, which was not statistically significant. We first considered a single-temperature, thin thermal plasma model (the APEC[24] code) with either 0.3 times solar metal abundances or solar composition and no foreground absorption. This model yielded a fit at above the 90% confidence level (reduced $\chi^2 = 0.91$, dof = 7). Assuming an elemental abundance of 0.3 solar, the plasma temperature was $kT = 0.25$ (0.22–0.29) keV, where the parentheses show the 90% confidence range. For solar abundances, $kT = 0.16$. For the reduced abundance model, $F_X \sim 4.2 \times 10^{-14}$ ergs cm$^{-2}$ s$^{-1}$ between 0.3 and 2 keV, corresponding to $L_X = 1.2 \times 10^{29}$ ergs s$^{-1}$. Our data can also be fit with a single-temperature, thin thermal plasma model with foreground absorption. In this case, we find $N_H \approx 5.4 \times 10^{20}$ cm$^{-2}$, and the *unabsorbed* $L_X = 1.5 \times 10^{29}$ ergs s$^{-1}$ (Fig. 11*a*). This luminosity is a factor of 5.7 lower than for the companions to HD 169142.

The $L_X$ value for HD 169142 is at the low end of the range observed for Herbig Ae stars (Fig. 11*b*; Hamaguchi et al. 2005; Swartz et al. 2005; Feigelson et al. 2003; Skinner 2004; Stelzer et al. 2006b) but is ≈$10^3$ higher than BPMG early- to mid-A stars (Hempel et al. 2005). The spectrum is also much softer than typical for accreting Herbig Ae stars, 10 times below the T Tauri companions above 1 keV, and most closely resembles BPMG early F stars such as 51 Eri (Feigelson et al. 2006; Stelzer et al. 2006a). The $L_X/L_{bol}$ value is also typical of early F stars. Our *Chandra* data suggest that HD 169142 has a magnetic field configuration similar to early F stars and is nonaccreting.

### 3.11. *Disk Structure Constraints*

Meeus et al. (2001) sorted Herbig Ae stars based on the appearance of their IR SEDs. HD 169142 was classified as a group Ib object. Meeus et al. interpreted these SEDs as arising in flared-disk systems. However, Whitney & Hartman (1992) found that an $r^{-3}$ radial surface brightness profile arises from a flat, geometrically

[24] See http://cxc.harvard.edu/atomdb/.

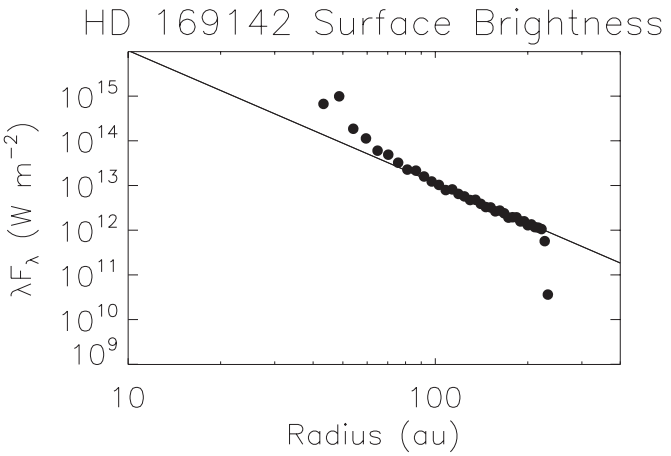


FIG. 12.—Radial surface brightness profile for models fitting the IR SED shows good agreement with the observed SB $\propto r^{-3}$ from 60 AU to the outer edge of the disk at 1.1 $\mu$m.

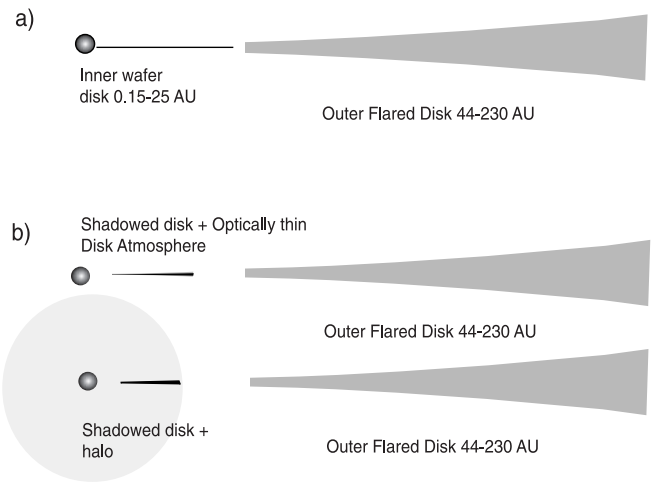


FIG. 13.—Simplified cartoons of the models that best fit the IR SED of HD 169142. (*a*) A wafer inner disk + flared outer disk, and (*b*) a shadowed inner disk with either an optically thin disk atmosphere or a disk halo, plus the flared outer disk.

thin, but optically thick disk. Dent et al. (2006) have modeled the disk using the library of D'Alessio et al. (2005) models (flared disks with gas and dust in hydrostatic equilibrium). To fit HD 169142, they need to (1) reduce the height of the dust disk at the sublimation temperature and (2) adopt $i = 30^\circ$ to avoid overestimating the flux in the NIR while (3) adopting $\dot{M}_{\rm acc} = 10^{-8}\ M_\odot\ {\rm yr}^{-1}$. Increasing the system inclination does indeed drop the mid-IR flux, but the coronagraphic and millimeter data firmly exclude inclinations higher than 20°. Moreover, at the high inferred mass accretion rate, a jet should be present, based on the behavior of other Herbig Ae stars, and conspicuous type I P Cygni profiles are expected in the UV, especially for an essentially pole-on viewing geometry. These features are not observed, suggesting that the disk modeling needs to be revisited.

To model the disk, we use the Whitney 3D Monte Carlo radiative transfer code (Whitney et al. 2003a, 2003b, 2004), which uses the radiative equilibrium method of Bjorkman & Wood (2001). A first step in this process is a more realistic treatment of the star. We model the flux density emerging from the stellar atmosphere as a linear combination of Kurucz models spanning 7800–4800 K. By doing so we achieve (1) a higher fidelity representation of the effect of gravity darkening, (2) an improved fit in the UV, and (3) a reduction in 1–2 $\mu$m excess otherwise attributed to the disk.

The NICMOS imagery, the polarimetric imagery (Kuhn et al. 2001), and the spatially extended PAH data (Habart et al. 2006) suggest that beyond 0.2″–0.3″ (29–44 AU) the outer disk is illuminated by the star and thus might be modeled as a flared disk, albeit with comparatively little flare, or one that is dominated by larger grains. A good fit to the IR SED, using $i = 10^\circ$, is achieved for a disk extending from 44 to 230 AU (Fig. 12). The grains used for this model are those used by Wood et al. (2002) to model HH 30 and consists of silicates and carbonaceous material, with a power-law plus exponential cutoff size distribution with a turnover at 50 $\mu$m radius and a maximum grain size of 1000 $\mu$m radius. This model has an illuminated wall at 44 AU with a half-height of 10 AU, where the dust density drops to $3 \times 10^{-6}$ of its midplane value. This corresponds to a minimum illumination angle for the outer disk of 2.2°. The outer disk intercepts 14% of the stellar luminosity. The disk structure is one that has minimal flaring, with a scale height increasing as $r^{+1.065}$, and with $r_{\rm in} = 44$ AU and $r_{\rm out} = 230$ AU. The model was adjusted to match the $r^{-3}$ radial surface brightness profile observed in the near-IR scattered light, but no attempt has been made to match the polarimetry. The current models employ scattering by spherical (Mie) particles, while real grains are likely to be porous aggregates whose scattering phase functions and polarization characteristics will be different. The location of the innermost wall is sensitive to the choice of grain size: *smaller* grains cause the location of the inner wall to move *outward*.

This disk model is essentially truncated at 44 AU, however, and cannot account for the small excess emission seen at $\lambda = 10$ $\mu$m. To meet the requirement of negligible outer disk shadowing, we have explored two models: one where the inner disk is treated as an optically thick, geometrically thin structure, or "wafer disk," and one where this portion of the disk is shadowed but may have an optically thin disk atmosphere (Fig. 13). In both cases, the inner edge of the disk, at the dust sublimation radius, produces emission that we treat as a blackbody. For the wafer disk model, we approximate the inner disk using the 1D DUSTY code (Nenkova et al. 2000). The best combined fit of this model and the Whitney flared outer disk is shown in Figure 14*a*, with an expanded scale detail of the near- to mid-IR region in Figure 14*b*. In this model the inner blackbody wall at $r = 0.15$ AU intercepts 7% of the starlight. The wafer disk intercepts/radiates 0.5% $L_*$, and has an $r_{\rm in} = 0.15$ AU and $r_{\rm out} = 5$ AU. Also shown is a model with the wafer extending to $r_{\rm out} = 40$ AU. Due to the glancing incidence angle of the stellar radiation in this model, extending this component has little effect on the mid-IR flux, changing it by less than 1%, but introduces some emission at millimeter wavelengths. In Figure 14*b* we illustrate the effect of removing the wafer component altogether. Here the solid lines include the wafer (it is insensitive as to the outer radius of this component) while the dotted curves are without the wafer entirely. The removal of this component only changes the flux by a few percent. The wafer disk is included in the model to allow for the possibility that some dust may occupy the midplane interior to the outer wall, but by no means can we prove its existence. The zone between the inner dust emission region represented by the blackbody in these models and the outer disk wall may, in fact, be relatively free of dust.

For the disk atmosphere model, we also treat the inner disk using DUSTY but approximate the disk atmosphere as a halo component. Vinković et al. (2003) have shown that mathematically

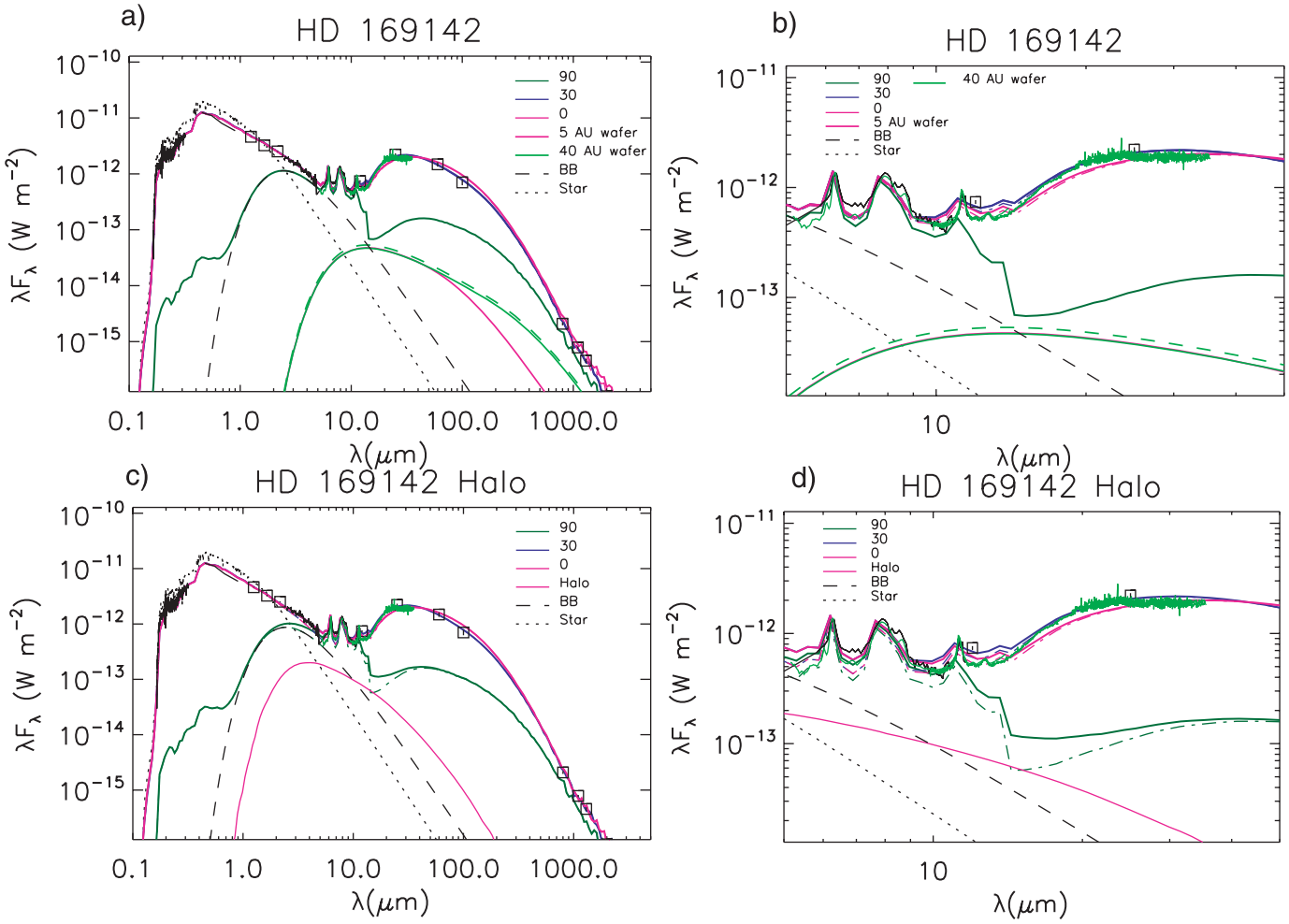


FIG. 14.—Fit to the IR SED of HD 169142. (*a*) The wafer inner disk + flared outer disk model. The data include IUE LWP 31285, SWP 55483, *BVRI* from van der Veen (1989), 2MASS photometry, *ISO* PHT40 data including both the phot40-short and phot40-long, *Spitzer* IRS ch0, ch1, and ch3, and millimeter data from Sylvester et al. (1996). At short wavelengths, the unreddened photospheric spectrum is shown as the black dotted curve, prior to correction by interstellar reddening ($A_V = 0.15$), and the inner blackbody component is the thick black dashed curve. (*a*) We illustrate the composite model SED produced by the Monte Carlo radiative transfer code (plus blackbody and wafer disk emission) for three inclinations: $i = 0°$ (*thin upper red curve*), 30° (*thin blue curve just below it*), and 90° (*thin dark-green curve*). The first two were chosen to effectively bracket the 11° inclination determined from the coronagraphic imaging, while including the 90° model demonstrates the maximum effect of changing the inclination from face-on (*red*) to equator-on (*green*) with the model. In these composite models, the wafer used had an outer radius of 40 AU (*lowest thin light-green line*). Above this (*thin dashed green line*) is the same wafer seen at 0° inclination, while the 90° would exhibit no observed flux and is not plotted. The thin magenta curve is the 30° wafer with an outer radius of only 5 AU. Due the grazing incidence of the stellar photons onto the wafers, extending the outer radius to 40 AU only contributes significantly to the longest wavelengths. The two thick dot-dashed curves passing through the data points are the same Monte Carlo models without the addition of the wafers, which add little observable emission between 20 and 100 $\mu$m, and only a small contribution near 10 $\mu$m. As seen in the figure, the SED is not very sensitive to the inclination for disks that are nearly face-on, so that its use in constraining the model should be avoided in such cases. (*b*) Detail of the wafer + outer flared disk model. (*c*) The fit for either the shadowed disk+disk atmosphere or halo and outer flared disk. The solid and dot-dashed lines are the models with and without the halo component, respectively. (*d*) Detail for the shadowed disk/halo + outer flared disk models.

the halo component in this model is equivalent to a disk atmosphere. In this case the inner disk wall intercepts 5% of the starlight and is located at 0.15 AU, while the disk atmosphere intercepts/radiates 1.2% $L_*$ with an $r_{in} = 0.15$ AU and an $r_{out} = 25$ AU. The model parameterization of this component in the spherical case has density $\propto r^{-2}$, which is equivalent to an optically thin disk with density $\propto r^{-1}$. Figure 14*c* shows the SED for the composite model using the disk atmosphere model for the inner disk and the Whitney flared outer disk, with an expanded scale in Figure 14*d*. Both models fit the data equally well, and both include species that are assumed to be in thermal equilibrium with the stellar radiation field. Since the PAH emission features are photoexcited, neither model constrains their location, which is known to arise over at least the inner 100 AU of the disk (Habart et al. 2006). As for the wafer + outer disk model, the inclusion of the halo component only affects the mid-IR emission at the level of a few percent at most, with no real contribution in the millimeter.

## 4. DISCUSSION

By $6^{+6}_{-3}$ Myr, HD 169142 has a disk with significant radial structure, and an absence of overt signatures of accretion expected from modeling of the outer disk (Dent et al. 2006; Garcia Lopez et al. 2006). The inner disk is flatter than the outer disk in both classes of models we have considered. The use of a blackbody in the DUSTY code is equivalent to the dust in this region being larger than 20 $\mu$m, suggesting that the inner disk either already has made, or is currently making, the transition to being a rubble disk. Both classes of models suggest that the inner disk may be decoupled from the outer, flared disk, naturally accounting for the low stellar accretion rate, in the presence of an outer disk retaining at least a minimum-mass solar nebula's

worth of gas and dust, as suggested by Raman et al. (2006) and Dent et al. (2006).

Several mechanisms can produce an inner disk structure differing from the outer disk, including (1) geometric shadowing (Dullemond & Dominik 2004a, 2004b), (2) grain growth in the inner disk that drops the dust opacity in this zone, and thus the observed IR excess out to 8–10 $\mu$m, (3) photoevaporation of the inner disk (Alexander et al. 2006), or (4) the presence of a second body in the disk that decouples the outer disk from the inner disk, with the inner disk subsequently draining onto the star. Geometric shadowing can modify the appearance of the IR SED but does not eliminate the UV excess light, wind features, or visibility of a jet or produce an X-ray spectrum typical of nonaccreting early F stars. While grain growth reduces the IR excess in the temperature range in which the large grains are present, it does not affect the presence of UV accretion signatures, since these are dominated by the gas. Moreover, at distances of a few $R_*$, where the UV excess light and the wind features are formed, all accreting material will be in the gas phase.

The two remaining possibilities are photoevaporation of the inner disk and the effect of a second body residing within the disk. Photoevaporation alone is expected to produce inner cavities in the disk, provided that the star (or other external sources) produce at least $10^{41}$ ionizing photons $s^{-1}$, and should result in complete clearing of the inner disk within $10^5$ yr (Alexander et al. 2006). Draining of the inner disk is expected when the outer disk mass is near 0.001 $M_\odot$. The removal of the gas in the inner disk then allows any remaining dust grains and larger bodies to settle into a flat disk (Cuzzi & Weidenschilling 2006). The estimated mass of HD 169142's outer disk between 0.02 and 0.04 $M_\odot$ is uncomfortably large for photoevaporation alone to have resulted in the flattening of the inner disk. Further, the short drain time would require that we view the star during an extremely short evolutionary phase. While this is always possible for any single object, one would expect the small number of Herbig Ae stars to sort into undrained, accreting systems, and objects resembling debris disks with transitional objects unobserved or very rare. However, the 40 Herbig Ae stars with high-quality *ISO* spectra (Acke et al. 2005), and the *HST* coronagraphically observed Herbig Ae stars, include several objects resembling HD 169142 in having wall structures an order of magnitude farther from the star than the drain radius predicted by the photoevaporation models. Thus, either photoevaporation alone is insufficient to account for the disk structure, or we live at an interesting time in an interesting part of the Galaxy.

A dynamical source for the difference between the inner and outer disks typically requires the presence of a second body within the disk. Low-mass stellar companions can be reliably identified via their X-ray fluxes and spectra, and with lower contrast to the central A star via their UV emission. No companion objects to HD 169142 were seen in close ($0.3'' < r < 1''$) proximity to the star in the NICMOS PSF-subtracted image. We assessed the companion detectability limits by implanting and recovering noiseless Tiny Tim model PSF template "stars" into the circumstellar region of HD 169142 in the presence of its disk, in the NICMOS PSF-subtracted coronagraphic image (see Lowrance et al. 2005). We found a robust 3 $\sigma$ detection limit for pointlike objects of F110W = 17.9 ($\Delta$F110W =10.6) at $1''$ and F110W = 16.2 ($\Delta$F110W = 8.9) at $0.6''$. Adopting a distance of 140 pc for HD 169142, and a color transformation for objects of likely late M to early L spectral type (as inferred from the luminosity difference) of $-0.3$ from NICMOS F110W to $J$ band, we find limiting $J$(abs) companion detection limits of 11.9 and 10.2 for $1.0''$ and $0.6''$ separations, respectively. The ACS F122M imagery firmly excludes the presence of any object more luminous than M3 V within the disk, exterior to $0.25''$. At $0.25''$ the detection limit is M2.5 V, and at $0.125''$ our detection limit is M0 V. Our *Chandra* data indicate that any source with a spectrum similar to the two T Tauri stars in the field must be 10 times less X-ray luminous, thus excluding a *stellar* coronal source down to M4.5 V. Nonaccreting brown dwarfs have spectra similar to HD 169142 at $t = 8$ Myr (Tsuboi et al. 2003), but are an order of magnitude fainter than the *Chandra* source at the location of the Herbig star. Thus, we cannot exclude the presence of a substellar X-ray source such as a brown dwarf within the disk of HD 169142. While wide star + brown dwarf binaries are known for both the TW Hya association and the BPMG (Feigelson et al. 2006; Stelzer et al. 2006a), none have been identified within 50 AU of a Herbig Ae primary and moreover *residing* within a protoplanetary disk, suggesting that any close companion to HD 169142 may be a planet.

## 5. SUMMARY

The disk of HD 169142 is detected in scattered light in the range $0.57'' \leq r \leq 1.4''$, in good agreement with polarimetric imaging and submillimeter observations. The disk has a steep, azimuthally medianed SB $\propto r^{-3}$. This distribution is similar to that of HD 100546, and intermediate between TW Hya and $\beta$ Pictoris. HD 169142 has previously been identified as a Meeus group I source, which can arise either from a flared disk or from a system with an internal cavity (Calvet et al. 2004) where the near-stellar dust has grown and settled to the midplane, and where the stellar radiation field has subsequently photodissociated the gas. Whitney & Hartmann (1992) find SB $\propto r^{-3}$ is produced by geometrically thin, optically thick disks, favoring the presence of a geometrically much flatter inner disk that may be decoupled from the outer disk. As Cuzzi & Weidenschilling (2006) note, this requires a low gas abundance in the inner disk. Several UV diagnostics indicate $\dot{M} \leq 10^{-9}\ M_\odot\ \mathrm{yr}^{-1}$. The inferred inner wall of the outer disk is an order of magnitude farther from the star than predicted by the current generation of photoevaporation models. Photoevaporation models also predict that the interval when the disk shows a distinct two-component structure should be a short-lived transition between a single disk and a debris disk. The presence of other similar stars in the comparatively small sample of stars with coronagraphic imaging and high-quality IR spectra suggests that other mechanisms, such as the presence of a second planetary or higher mass body, may be required. For HD 169142, our data exclude any *stellar* companion within $1''$ of the primary as the source of the radial structure.

Combining the system inclination with previously published $v \sin i$ data leads to the conclusion that HD 169142 is an extremely rapidly rotating star. We find, in the trend of systematically later inferred FUV spectral type compared to the optical type, evidence for gravity darkening, similar to that seen for Altair. A late A-type star such as HD 169142 will retain at least a shallow convective zone throughout its main-sequence lifetime; the enhanced X-ray and UV line emission may reflect rotational enhancement of chromospheric and transition region activity. The same rapid rotation may account for prior identification of this star as chemically peculiar; a more detailed modeling of the spectrum expected from a star exhibiting a large pole-to-equator temperature gradient is needed before departures from solar composition can be confirmed. Since rapid rotators are not expected to show the chemical peculiarities seen in slowly rotating stars, any true abundance deficits should reflect the composition of the parent molecular cloud. By combining a

pole-on viewing geometry and rapid rotation, HD 169142 offers a view of what a younger Vega may have looked like.

This work is based in part on observations made with the NASA/ESA *Hubble Space Telescope*, obtained at the Space Telescope Science Institute, which is operated by the Association of Universities for Research in Astronomy (AURA), Inc., under NASA contract NAS5-26555. Support for these programs was provided by NASA through a grant from the Space Telescope Science Institute, which is operated by AURA under NASA contract NAS5-26555 as part of HST-GO-10177 and HST-GO-10764. This work is also based on observations made with the *Chandra X-Ray Observatory* under program P7200493. Support for this work was provided by NASA through Chandra awards G06-7010A and G06-7010B issued by the *Chandra* Center, which is operated by the Smithsonian Astrophysical Observatory for and on behalf of NASA under contract NAS8-03060. Observing time at the Apache Point Observatory 3.5 m for the Goddard Fabry-Perot was provided by a grant of Director's Discretionary Time. Time for the DIS spectra was awarded through the JHU time allocation. Apache Point is operated by the Astrophysical Research Consortium. The Goddard Fabry-Perot is supported under NASA RTOP 51-188-01-22 to GSFC. C. A. G. is also supported as part of the Astrophysics Data Program under NASA contract NNH06CC28C to Eureka Scientific, HST-GO-10177.02-A, HST-GO-10764.01-A, and Chandra G06-7010A. G. S. is supported under HST-GO-10177.01. K. H. is supported by *Chandra* US grants (GO3-4008A, GO6-7010B). M. L. S. is supported through the NASA Origins of Solar Systems Program grants NAG5-9475 and NAG5-13242, NASA Astrophysics Data Program contract NNH05CD30C, and HST-GO-10764. K. A. C. is supported by a Kentucky Space Grant Consortium Fellowship under NASA National Space Grant College and Fellowship Program grant NNG05GH07H. Data analysis facilities were provided by the Steward Observatory of the University of Arizona and the Astrophysical Systems Division at NASA's GSFC. We thank the anonymous referee whose comments improved the paper.

*Facilities:* HST (NICMOS), HST (ACS), CXO(ACIS-S), ARC

REFERENCES

Acke, B., & van den Ancker, M. E. 2004, A&A, 426, 151
Acke, B., van den Ancker, M. E., & Dullemond, C. P. 2005, A&A, 436, 209
Alexander, R. D., Clarke, C. J., & Pringle, J. E. 2006, MNRAS, 369, 229
Aufdenberg, J. P., et al. 2006, ApJ, 645, 664
Augereau, J.-C., Lagrange, A. M., Mouillet, D., & Ménard, F. 2001, A&A, 365, 78
Augereau, J.-C., & Papaloizou, J. C. B. 2004, A&A, 414, 1153
Baraffe, I., Charbrier, G., Allard, F., & Hauschildt, P. H. 1998, A&A, 337, 403
Bjorkman, J. E., & Wood, K. 2001, ApJ, 554, 615
Calvet, N., Muzerolle, J., Briceño, C., Hernández, J., Hartmann, L., Saucedo, J. L., & Gordon, K. D. 2004, AJ, 128, 1294
Carmona, A., van den Ancker, M. E., & Henning, T. 2007, A&A, 464, 687
Chen, X. P., Henning, T., van Boekel, R., & Grady, C. 2006, A&A, 445, 331
Collins, K. A., et al. 2007, Detection of Optical Ghost in *HST* ACS Solar Blind Channel Filter 122M (ACS Instrument Science Rep. 2007-0005; Baltimore: STScI)
Cuzzi, J. N., & Weidenschilling, S. J. 2006, in Meteorites and the Early Solar System II, ed. D. S. Lauretta & H. Y. McSween (Tucson: Univ. Ariz. Press), 353
D'Alessio, P., Merín, B., Calvet, N., Hartmann, L., & Montesinos, B. 2005, Rev. Mex. AA, 41, 61
Dent, W. R. F., Greaves, J. S., & Coulson, I. M. 2005, MNRAS, 359, 663
Dent, W. R. F., Torrelles, J. M., Osorio, M., Calvet, N., & Anglada, G. 2006, MNRAS, 365, 1283
Devine, D., Grady, C. A., Kimble, R. A., Woodgate, B., Bruhweiler, F. C., Boggess, A., Linsky, J. L., & Clampin, M. 2000, ApJ, 542, L115
Domiciano de Souza, A., Kervella, P., Jankov, S., Vakili, F., Ohishi, N., Nordgren, T. E., & Abe, L. 2005, A&A, 442, 567
Dullemond, C. P. E., & Dominik, C. 2004a, A&A, 417, 159
———. 2004b, A&A, 421, 1075
Dunkin, S. K., Barlow, M. J., & Ryan, S. G. 1997a, MNRAS, 286, 604
———. 1997b, MNRAS, 290, 165
Endres, M., Haddad, N., Hilton, G. M., Grady, C. A., Woodgate, B. E., & Williger, G. M. 2005, BAAS, 37, 1287
Feigelson, E. D., Lawson, W. A., & Garmire, G. P. 2003, ApJ, 599, 1207
Feigelson, E. D., Lawson, W. A., Stark, M., Townsley, L., & Garmire, G. P. 2006, AJ, 131, 1730
Garcia Lopez, R., Natta, A., Testi, L., & Habart, E. 2006, A&A, 459, 837
Garmire, G. P., Bautz, M. W., Ford, P. G., Nousek, J. A., & Ricker, G. R., Jr. 2003, Proc. SPIE, 4851, 28
Gelderman, R., Woodgate, B. E., & Brown, L. 1995, in IAU Colloq. 149, Tridimensional Optical Spectroscopic Methods in Astrophysics, ed. G. Comte & M. Marcelin (ASP Conf. Ser. 71; San Francisco: ASP), 89
Golimowski, D. A., Durrance, S. T., & Clampin, M. 1993, ApJ, 411, L41
Gonzaga, S., et al. 2005, ACS-SBC-DITHER-BOX Pointing Patterns (Baltimore: STScI), http://www.stsci.edu/hst/acs/proposing/dither/ACS-SBC-DITHER-BOX.html
———. 2006, ACS Instrument Handbook, Version 6.0 (Baltimore: STScI)
Grady, C. A., et al. 1996, A&AS, 120, 157
———. 2001, AJ, 122, 3396
Grady, C. A., et al. 2004, ApJ, 608, 809
Habart, E., Natta, A., Testi, L., & Carbillet, M. 2006, A&A, 449, 1067
Hales, A. S., Gledhill, T. M., Barlow, M. J., & Lowe, K. T. E. 2006, MNRAS, 365, 1348
Hamaguchi, K., Yamauchi, S., & Koyama, K. 2005, ApJ, 618, 360
Hartmann, L. 2005, in ASP Conf. Ser. 337, The Nature and Evolution of Disks Around Hot Stars, ed. R. Ignace & K. G. Gayley (San Francisco: ASP), 3
Hempel, M., Robrade, J., Ness, J.-U., & Schmitt, J. H. M. M. 2005, A&A, 440, 727
Houck, J. R., et al. 2004, Proc. SPIE, 5487, 62
Kirkpatrick, J. D., Henry, T. J., & McCarthy, D. W., Jr. 1991, ApJS, 77, 417
Kuhn, J. R., Potter, D., & Parise, B. 2001, ApJ, 553, L189
Lowrance, P. J., et al. 1999, ApJ, 512, L69
———. 2005, AJ, 130, 1845
Meeus, G., Waters, L. B. F. M., Bouwman, J., van den Ancker, M. E., Waelkens, C., & Malfait, K. 2001, A&A, 365, 476
Nenkova, M., Ivezić, Ž., & Elitzur, M. 2000, in ASP Conf. Ser. 196, Thermal Emission Spectroscopy and Analysis of Dust, Disks, and Regoliths, ed. M. L. Sitko, A. L. Sprague, & D. K. Lynch (San Francisco: ASP), 71
Peterson, D. M., et al. 2006a, ApJ, 636, 1087
———. 2006b, Nature, 440, 896
Raman, A., Lisanti, M., Wilner, D. J., Qi, C., & Hogerheijde, M. 2006, AJ, 131, 2290
Roberge, A., et al. 2001, ApJ, 551, L97
Schneider, G., Silverstone, M. D., & Hines, D. C. 2005, ApJ, 629, L117
Schneider, G., & Stobie, E. 2002, in ASP Conf. Ser. 281, Astronomical Data Analysis Software and Systems XI, ed. D. A. Bohlender, D. Durand, & T. H. Handley (San Francisco: ASP), 382
Schneider, G., et al. 2001, AJ, 121, 525
———. 2006, ApJ, 650, 414
Skinner, S. L., Güdel, M., Audard, M., & Smith, K. 2004, ApJ, 614, 221
Sloan, G. C., et al. 2005, ApJ, 632, 956
Stauffer, J. R. 2004, in ASP Conf. Ser. 324, Debris Disks and the Formation of Planets, ed. L. Caroff, L. J. Moon, D. Backman, & E. Praton (San Francisco: ASP), 100
Stecklum, B., et al. 2007, A&A, in press
Stelzer, B., Micela, G., Flaccomio, E., Neuhäuser, R., & Jayawardhana, R. 2006a, A&A, 448, 293
Stelzer, B., Micela, G., Hamaguchi, K., & Schmitt, J. H. M. M. 2006b, A&A, 457, 223
Strom, S. E., & Najita, J. 2005, in Protostars and Planets V (LPI Contrib. 1286; Houston: LPI), 8078
Swartz, D. A., Drake, J. J., Elsner, R. F., Ghosh, K. K., Grady, C. A., Wasell, E., Woodgate, B. E., & Kimble, R. A. 2005, ApJ, 628, 811
Sylvester, R. J., Skinner, C. J., Barlow, M. J., & Mannings, V. 1996, MNRAS, 279, 915
Tsuboi, Y., Maeda, Y., Feigelson, E. D., Garmire, G. P., Chartas, G., Mori, K., & Pravdo, S. H. 2003, ApJ, 587, L51
van Boekel, R. Waters, L. B. F. M., Dominik, C., Bouwman, J., de Koter, A., Dullemond, C. P., & Paresce, F. 2003, A&A, 400, L21

van der Veen, W. E. C. J., Habing, H. J., & Geballe, T.R. 1989, A&A, 226, 108
Vinković, D., Ivezić, Ž., Jurkić, T., & Elitzur, M. 2003, MNRAS, 346, 1151
Voges, W., et al. 1999, A&A, 349, 389
Walker, H. J., & Wolstencroft, R. D. 1988, PASP, 100, 1509
Wassell, E. J., Grady, C. A., Woodgate, B., Kimble, R. A., & Bruhweiler, F. C. 2006, ApJ, 650, 985
Weinberger, A. J., Rich, R. M., Becklin, E. E., Zuckerman, B., & Mathews, K. 2000, ApJ, 544, 937
Weinberger, A. J., et al. 2002, ApJ, 566, 409
Werner, M., Giovanni, F., Rieke, G., Roellig, T. L., & Watson, D. M. 2006, ARA&A, 44, 269
Whitney, B. A., & Hartmann, L. 1992, ApJ, 395, 529
Whitney, B. A., Indebetouw, R., Bjorkman, J. E., & Wood, K. 2004, ApJ, 617, 1177
Whitney, B. A., Wood, K., Bjorkman, J. E., & Cohen, M. 2003a, ApJ, 598, 1079
Whitney, B. A., Wood, K., Bjorkman, J. E., & Wolff, M. J. 2003b, ApJ, 591, 1049
Wood, K., Wolff, M. J., Bjorkman, J. E., & Whitney, B. A. 2002, ApJ, 564, 887
Zuckerman, B., & Song, I. 2004, ARA&A, 42, 685